

## **Micrometer and nanometer size platinum group nuggets in micrometeorites from the deep sea sediments of Indian Ocean**

N.G. Rudraswami, K. Parashar and M. Shyam Prasad\*

National Institute of Oceanography (Council of Scientific and Industrial Research),  
Dona Paula, Goa 403004, INDIA

\*Corresponding author, Tel: +91-9423056118, Fax: +91-832-2450602,

E-mail: shyam@nio.org

### **ABSTRACT**

We examined 378 micrometeorites collected from deep sea sediments of Indian Ocean of which 175, 180 and 23 are I-type, S-type and G-type, respectively. Of the 175 I-type spherules, thirteen contained platinum group element nuggets (PGN). The nuggets occur in two distinct sizes and have distinctly different elemental compositions: micrometer ( $\mu\text{m}$ ) sized nuggets that are greater than  $3 \mu\text{m}$  contain dominantly Ir, Os, and Ru (iridium-platinum group element or IPGE) and sub- $\mu\text{m}$  (or nanometer) sized ( $< 1 \mu\text{m}$ ) nuggets which contain dominantly Pt, Rh and Pd (Palladium-PGE or PPGE). The  $\mu\text{m}$  sized nuggets are found only one per spherule in the cross-section observed and are usually found at the edge of the spherule. In contrast, there are hundreds of nanometer sized nuggets distributed dominantly in the magnetite phases of the spherules, and rarely in the wustite phases. Both the nugget types are found as separate entities in the same spherule and apparently, nugget formation is a common phenomenon among I-type micrometeorites. However the  $\mu\text{m}$  sized nuggets are seen in fewer specimens ( $\sim 2.5\%$  of the observed I-type spherules). In all we analysed four nuggets of  $\mu\text{m}$  size and two hundred thirteen nanometer sized nuggets from thirteen I-type spherules for platinum group elements.

Chemically, the  $\mu\text{m}$  sized PGNs contain chondritic ratios of Os/Ir, but are depleted in the more volatile PGE (Pt, Rh and Pd) relative to chondritic ratios. On the other hand, the nanometer sized nuggets contain dominantly Pt and Rh. Importantly, the refractory PGE are conspicuous by their absence in these nanometer nuggets. Palladium, the most volatile PGE is highly depleted ( $< 1.1\%$ ) with respect to chondritic ratios in the  $\mu\text{m}$  sized PGNs, and is observed in only 17 out of 213 nanometer nuggets with concentrations which are just above the detection limit ( $\geq 0.2\%$ ). Distinct fractionation of the PGE into IPGE (Ir, Os, Ru) and PPGE, seems to take place during the short span of atmospheric entry.

These observations suggest several implications: (1) The observation of fractionated PGE in an Fe-Ni system, gives rise to the possibility that the Earth's core could contain fractionated PGE. (2) The present data supports the processes suggested for the fractionated PGE patterns observed in the ejecta of ancient meteorite impacts. (3) Meteoric metals released in the troposphere could contain fractionated PGNs in large numbers.

**Keywords:** cosmic spherules, platinum group element, nuggets, parent body, chondrites, impact craters

## INTRODUCTION

Micrometeorite flux on the Earth is estimated at  $\sim 30,000$  tons/year by different methods (Love and Brownlee 1993; Peucker-Ehrenbrenk and Ravizza 2000). Several thousands of extraterrestrial particles have been collected from various environments all over the Earth (Bruun et al. 1955; Millard and Finkelman 1970; Brownlee et al. 1979; Blanchard et al. 1980; Maurette et al. 1986, 1991; Taylor et al. 2000), and from the stratosphere as well (Brownlee et al. 1977). Brownlee (1985) estimated that a million micrometeorites had been isolated from all known environments two and half decades ago. This number would of course, be much larger today.

Micrometeorites of sizes  $> 50 \mu\text{m}$  undergo melting during atmospheric entry (Love and Brownlee 1993). The melting of this material depends on composition of the parent body, angle of entry, entry velocity, and the physical properties of the incoming particle (Brownlee 1985). Three broad micrometeorite types have been recognized: S-type, I-type and the G-type. All the three could have the same parent body - a carbonaceous chondrite (Brownlee et al. 1997). They are generated because of differences in their processing during atmospheric entry. Alternatively, the presence of cosmogenic radionuclides indicated that the I-type spherules could be atmospherically processed metal grains from carbonaceous /unequilibrated chondritic bodies (Herzog et al. 1999). Variation in the atmospheric entry parameters (entry velocity, angle, chemical composition, size and physical properties) lead to different stages and levels of melting. Different stages of melting have been characterized in the S-type spherules and have been classified from the least melted scoriaceous to the most refractory CAT spherules which indicate increasing heating, and progressive volatilization of Fe (Taylor et al. 2000; Genge et al. 2008).

Brownlee et al. (1984) discovered Pt-group nuggets of micrometer ( $\mu\text{m}$ ) sizes in a small percent of I-type spherules. They proposed that these nuggets are the products of extreme levels of oxidation and heating of a chondritic parent body, and the elemental fractionation observed in these nuggets are suggestive of an unfractionated chondritic parent body. Furthermore, Bonte et al. (1987) discovered both  $\mu\text{m}$  and nanometer sized nuggets in both I-type and also for the first time, in an S-type spherule. They further suggested that the presence of such nuggets in an S-type spherule implies that a single process such as the extreme heating and oxidation of a chondritic parent body may not be the only process involved in the formation of nuggets because, the fractionation patterns of Ir, Fe, Ni, Co and Sc indicated an iron-rich parent body with a minor fraction of chondritic material.

We made a large collection of extraterrestrial matter from the deep sea floor of the Central Indian Ocean by (1) raking the sea floor with a dredge fitted with magnets and; (2) magnetic

separation from deep sea sediments which were collected with a grab sampler. Examination of these collections led us to the finding of  $\mu\text{m}$  and nanometer sized PGNs in I-type spherules. These nuggets which show distinct fractionation of the PGE further provide insight into atmospheric entry processes, PGE fractionation in differentiated planets and PGE signatures in meteorite impact craters.

## **SAMPLING AND ANALYTICAL TECHNIQUES**

The samples were collected during the 22<sup>nd</sup> (AAS-22: Oct-Nov. 1999), 26<sup>th</sup> (AAS-26: April-May 2000) and 38<sup>th</sup> (AAS-38: May-June, 2001) cruises of AA Sidorenko, a research vessel chartered by the Government of India. During the first two cruises (AAS-22 and AAS-26) a massive (> 500 kg) dredge was dragged along the deep sea floor (water depth  $\sim$  5200 m) of the Central Indian Ocean for the bulk collection of polymetallic nodules. On one of the walls of this dredge an assembly comprising an aluminium panel over which bar magnets of 1400 gauss intensity were fixed. On these magnets a non-magnetic mesh wire was fixed and on the mesh wire a nylon cloth was put. Over this assembly, clamps were fixed on the borders and the entire assembly was clamped to a wall of the dredge. When the dredge was dragged along the seafloor, this assembly came into contact with the ploughed deep sea sediment, and the magnetic material that was attracted to this assembly was removed once the dredge was onboard. Each such sampling operation (i.e., lowering of the dredge, dragging on the seafloor and hauling up) took 12 hours. During AAS-22 we could carry out 14 such operations, whereas in AAS-26 we carried out 45 successful sampling operations. These operations, procedure for separation of spherules etc. are essentially similar to the ones presented in Parashar et al. (2010). In the present study, we examined spherules isolated from eleven operations (five from AAS-22 and six from AAS-26).

In addition, 25 kg of deep seafloor sediment from the Central Indian Ocean was collected using a grab sampler (AAS-38/139) which was sieved onboard with a 220  $\mu\text{m}$  mesh size sieve. The dried material > 220  $\mu\text{m}$  was subjected to magnetic separation and we recovered close to 50 micrometeorites, out of which two are I-type spherules. One of the spherules is nugget-bearing and was analyzed in this study. From all the above collections, we examined and characterized 378 spherules out of which 175, 180, 23 were I-, S- and, G-types, respectively, as shown in Table 1. Investigation of the 175 I-type spherules led to the discovery of four  $\mu\text{m}$  as well as two hundred and thirteen nanometer sized Pt-group nuggets (PGN) from thirteen I-type spherules (Table 2).

For preliminary observations, the spherules were mounted on stubs to study the external morphology. These spherules were subsequently mounted in epoxy and polished sections were

obtained. Through microscopic examination we identified one Pt-group nugget which was sitting on the surface of an I-type spherule (Figs. 1A and 1B). On a larger scale, the spherules were mounted in epoxy directly and their polished sections were obtained. The polished spherules were initially documented and photographed using an optical microscope. The sections were then coated with carbon and were analysed in a JEOL JSM-5800 LV Scanning Electron Microscope (SEM) and an OXFORD INCA EDS analytical system attached to the SEM.

Pure Pt-group element (99.9%) standards were used and data are quantified using ZAF methods which convert the x-ray intensity to concentration. The L and M series lines were used for the PGE. The uncertainty in the EDS analysis depends on the concentration of the element present in the nugget. Generally the uncertainty was found to be less than 10 % when concentration of the element was  $> 7$  wt %. However, in elements like Pd and Rh which had low concentrations, the error percentage was higher (up to  $\sim 30$  %). Quantitative optimization and nominal calibration were carried out routinely for a reliable outcome. Also the identification and resolving of the closely overlapping lines of elements like Ru, Rh and Pd was confirmed and tested with the standards repeatedly. The cosmic spherules could be easily distinguished from the terrestrial ones, especially in the backscattered electron image mode using the criteria established by Blanchard et al. (1980) and other investigators. We identified thirteen spherules that contain Pt-group nuggets having a size range of  $\sim 100$  nanometers to  $4.9 \mu\text{m}$ . The larger  $\mu\text{m}$  sized nuggets were visible under magnifications of 100X or more, while for the small i.e.,  $< 1 \mu\text{m}$  sized nuggets, magnifications up to 70,000X were used during analysis. The spherules hosting the nuggets basically consisted of varying combinations of magnetite and wustite. Further, chemical analysis was done with a CAMECA SX-100 electron probe microanalyzer (EPMA) to derive the compositions of magnetite and wustite. The parameters used were: accelerating voltage of 15 kV, and 15 nA sample current, PAP corrections were made with an online program (Pouchou and Pichoir 1991). The EPMA could not be used for the  $\mu\text{m}$  and nanometer sized nuggets because the beam size (1 - 2  $\mu\text{m}$  in diameter) is larger than the diameters of all the nuggets.

## RESULTS

### Description of Nuggets

We identified four  $\mu\text{m}$  sized nuggets and two hundred and thirteen nanometer nuggets from thirteen I-type spherules. All the nugget-bearing spherules are of the I-type. The spherules have a combination of magnetite and wustite in varying percentages however, in the nugget-bearing spherules, magnetite content is dominantly higher and all the spherules contain a magnetite rim as

well. Wustite is a metastable iron mineral ( $\text{Fe}_{(1-x)}\text{O}$ ) which forms under low oxygen partial pressure during atmospheric entry (Brownlee et al. 1975). Brownlee et al. (1984) and Bonte et al. (1987) after discovering Pt-group nuggets in individual spherules, systematically polished these spherules at micrometer levels and observed them under the SEM sequentially. While Brownlee et al. (1984) found that the spherules could contain only one, Bonte et al. (1987) found more than one  $\mu\text{m}$  sized nugget per spherule. Both these investigating groups found  $\mu\text{m}$  sized nuggets in the magnetite portions of the spherules. Brownlee et al. (1984) found nuggets in I-type spherules which had diameters  $> 300 \mu\text{m}$ , whereas Bonte et al. (1987) found them in smaller spherules as well (100 - 500  $\mu\text{m}$  diameter range). Feng et al. (2005) reported on the presence of likely nuggets in I-type spherules based on x-ray computed tomographic analyses.

### **Micrometer sized nuggets**

The  $\mu\text{m}$  sized nuggets are spherical in outline, and are found near the edge of the spherules in all the cases (Fig. 1). In one spherule AAS26-D1-Hh, the nugget was found on the surface of the spherule (Figs. 1A and 1B). The diameters of the  $\mu\text{m}$  sized nuggets found here are: 4.9, 4.5, 3.3 and 3.6  $\mu\text{m}$  (Fig. 1 and Table 3). Quite significantly, in the cross-sections of the spherules observed, two of the spherules (AAS 26-D1-P8 and AAS 22-D3-P4) contain both  $\mu\text{m}$  and nanometer nuggets (Fig. 2B, see also Table 4). Here, the  $\mu\text{m}$  sized nuggets are found close to the edge of the spherule, whereas the nanometer nuggets are found scattered, but confined to the magnetite portions of the spherules.

### **Nanometer nuggets**

Nanometer sized nuggets are to a large extent (i.e.,  $> 80\%$ ) spherical in shape, however some nuggets have shapes of teardrops, or are elongated, but are basically variants of a sphere (Figs. 2, 3 and 4). Magnifications up to 50,000 to 70,000X were used to identify even the smallest nugget. These are found dominantly in the magnetite grains of the spherules, however, in some spherules Pt-enriched ( $\text{Pt} \leq 1\%$ ) nuggets were also found in the wustite portions (Figs. 4 and 5).

#### *Nanometer nuggets in magnetite grains*

In the magnetite portions the nanometer sized nuggets stand out especially in the backscattered electron (BSE) image mode of the SEM (Fig. 3). They have spherical shapes. However, Bonte et al. (1987) reported angular shapes of such small nuggets which they suggested could be primary shapes. The nanometer nuggets in magnetites occur as discrete nuggets in the grains and sometimes more than one such nugget is found in individual magnetite grains (Figs. 2 and

3). Nine spherules contained nanometer sized nuggets, the number of nuggets in these spherules varied from 1 to 104. (Appendix 1 and Table 4). This clearly implies that there could have been several more nanometer sized nuggets in all these spherules. The diameters measured for 213 nanometer nuggets varies from 95 to 762 nanometers with an average diameter of 273 ( $\pm 117$ ) nanometers. In the spherule AAS-26-D1-#2- P1 the spatial density of nanometer sized PGNs is 0.0025 per square  $\mu\text{m}$ . In all, a total of 213 discrete nuggets are observed (Table 2). In addition, there are also nugget ‘chains’ in magnetites, which are basically Ni-rich. Some of these chains appear to lead to a larger, brighter (in the backscattered image) nugget which contains Pt in low quantities (Figs. 5 A, 5B and 5C). In general many magnetite grains contain Ni-rich ‘nuggets’ at the grain borders. Only the discrete nuggets in magnetite grains contain larger percentages of Pt (up to 24 %), and show the presence of Rh and rarely, other PGE (Table 2).

#### *Nanometer nuggets in wustite grains*

While high Pt nanometer nuggets in magnetites occur as discrete nuggets, such discrete nuggets in wustites are very rare (Fig. 4). The nanometer nuggets in wustite grains mostly occur as chains which are generally Ni-rich (Figs. 2C and 5). The nuggets in these chains contain progressively increasing quantities of nickel, which would further lead to nuggets which contain detectable quantities of Pt (Figs. 4 and 5). The Pt content in such nuggets is always low ( $< 1\%$ ). Although several hundreds of nanometer nuggets are seen in wustite grains, only a few of these appear to contain detectable quantities of Pt.

Interestingly, the nugget chains are observed in those spherules which have the least numbers of discrete nuggets. For example, in AAS-26-D1-#2-P1 which has 104 discrete nuggets (Table 2; Fig. 2A), nugget chains are absent. The chains are more profusely distributed within the spherules in AAS-26-D1-P8, AAS-38-139-#1-P20, AAS-26-D1-#2- P5 which otherwise have only 5, 1, and 1 discrete nuggets, respectively (Table 2; Fig. 5).

Brownlee et al. (1984) reported only  $\mu\text{m}$  sized nuggets, whereas Bonte et al. (1987) reported nanometer sized PGNs in both I-type and also in one rare S-type spherule. They found the nanometer nuggets dispersed in the magnetite phase of the spherules, and suggested that these nuggets were ‘disequilibrated’ because these nuggets contained only volatile PGE and were depleted in the more refractory PGE such as Os and Ir. Some of these nuggets were described to have a geometrical habit. Further, Bonte et al. (1987) described ‘tiny and needle-shaped segregations of Ni’ which probably are similar to the Ni-rich and Pt-rich nuggets as seen in Figs. 5A and 5C. More interestingly, the

nanometer sized nuggets found by Bonte et al. (1987) in the S-type spherule were associated with magnetite and these nuggets contained varying proportions of PGE.

### **Chemical composition of nuggets**

There is distinct difference in the compositions of the  $\mu\text{m}$  and the nanometer sized nuggets.

#### *Micrometer sized nuggets*

These nuggets contain very high percentages of the refractory PGE, Os and Ir (Os range: 18.3-50.8; Ir range 20.5-37.3), they also contain most or all of the Pt-group elements in lesser quantities. The refractory PGE such as Os, Ir have refractory properties as metals and osmium is volatile as an oxide, however, for the pressure at which the spherules form ( $<10^{-5}$  atm) oxidation of Os can take place only under temperatures  $< 600^{\circ}\text{C}$  (Brownlee et al. 1984). Whereas, by the time the spherule cools to this temperature, the nugget would have been encased in solid iron oxide (Brownlee et al. 1984). The four  $\mu\text{m}$  sized nuggets observed in the spherules AAS-26-D1#1-P8, AAS-26-D1-#1- P9, AAS-26-D1-Hh and AAS22-D3-P4 have diameters of 4.9, 4.5, 3.3, 3.6  $\mu\text{m}$ , respectively. Of these, AAS-26-D1-P8 and AAS-26-D1-Hh contain all the six Pt-group elements. The AAS-26-D1-#1P9 do not show Pt contents, while the AAS-22-D3-P4 does not contain Rh and Pd (Table 3). AAS-26-D1-P8 does have lesser amount of Pd compared to AAS-26-Hh, but all the other Pt-group elements are present (Table 3). In the nanometer sized nuggets, apparently the more volatile Pt-group elements or the PPGE (Palladium-PGE: Pt, Ru and, Rh) are either depleted or totally absent. However, the largest of the nuggets (AAS-26-D1-P8) shows up high enrichment in volatile as well as refractory PGE: Os (18.3%), Ir (20.5 %), Pt (17.7 %), Ru (17.6 %), Rh (1.9 %) and Pd (0.4 %). Brownlee et al. (1984) suggested that if the heating of the micrometeorite during atmospheric entry is not severe, then comparatively volatile elements such as Rh, Ni and Pd would be retained. The retention of the volatile PGE in this spherule (AAS-26-D1-P8) could, therefore indicate that it may not have experienced extreme heating.

If one considers a carbonaceous chondrite as a parent body for these micrometeorites as suggested by Brownlee et al. (1984) in view of their fractionation patterns, then, it would be by taking into account either the bulk composition or they are derived from PGE nuggets encountered in the CAIs of CI chondrites (Palme and Wlotzka 1976). Brownlee et al. (1984) ruled out the latter possibility because of the larger sizes and more frequent occurrence of the nuggets found in spherules.

Therefore, these nuggets may represent processed bulk carbonaceous chondritic material. Alternatively, I-type spherules, which in the present study host PGNs, could have also originated from unequilibrated ordinary chondrites (Herzog et al. 1999). Furthermore, the nuggets could have also originated from an iron-rich parent body with a minor fraction of chondritic material as shown by fractionation patterns of Ir, Fe, Ni, Co and Sc (Bonte et al. 1987). The fractionation patterns defined by all the nuggets found so far in the micrometer size range (Fig. 6) (i.e., including those analysed by Brownlee et al. (1984); and Bonte et al. (1987)) also show progressive depletion of the volatile PGE from an unfractionated chondritic parent body. If one considers the CI elemental ratios for PGE as shown in Table 5 (Tagle and Berlin 2008), two nuggets in the present collection show Os/Ir (normalized to CI) close to unity, whereas in AAS-22-D3-P4 the Os/Ir ratio is  $\sim 1.45$  and in AAS-26-D1-Hh the ratio is 0.72. The Os/Ir ratios of the latter two samples do not fall within the chondritic range (Fig. 9), but they are within the range ascertained for iron meteorites. However, the Os/Ir range for all chondritic meteorites is quite narrow and can be considered as diagnostic, whereas the range of Os/Ir ratios in iron meteorites is extremely large, therefore the uncertainties in assigning an iron meteorite parent body are also quite large.

Further, Ru/Ir ratios of these nuggets are much below the chondritic value of  $\sim 1.5$  and show values of 0.86, 0.39, 0.61, 0.31 for AAS-26-D1- P8, AAS-26-D1-#1- P9, AAS-26-D1-Hh and AAS22-D3-P4, respectively, because of Ru depletion in these nuggets. Similarly, although Pt is seen in good percentages in two out of the four nuggets (17.5 and 6.4 % in AAS-26-D1#1-P8 and AAS-22-D3-P4, respectively), it is below detection limit in the other two (AAS-26-D1-#1-P9 and AAS-22-D3-P4). Whereas, when we look at the elemental ratios in the nuggets of AAS-26-D1-P8 and AAS-26-D1-Hh where Pt is present, we see, Pt/Ir = 0.87 and 0.19, and Pt/Os= 0.97 and 0.27, respectively, which are much below the CI chondritic average of 2.03 and 1.97 (for Pt/Ir and Pt/Os) because of large scale depletion of Pt in these nuggets. Furthermore, Pt/Ru and Pt/Rh ratios of CI chondrites are 1.34 and 7.12, respectively (Tagle and Berlin 2008). These ratios when compared with the data show: Pt/Ru = 1.01 and 0.32 in two of the nuggets where Pt is present, and, Pt/Rh ratios are: 9.32 and 4.46 (see Table 5). Whereas among the volatile PGEs, Pd is observed in rare cases that too in very small percentages (i.e., less than 0.5 % except in one case where it was 1.1 %) and Rh is present only in small quantities (1.9 % and 1.4 %) in two of the nuggets.

Overall, in the  $\mu\text{m}$  sized PGNs, it appears that the refractory IPGEs (especially Os and Ir) are enriched and are present in near chondritic ratios. Ru is present in quantities that are lesser than chondritic averages, but the PPGEs (i.e., Pt, Rh and Pd) are either absent or are largely depleted (Figs. 6 and 7). If one looks at the nuggets analysed by Brownlee et al. (1984) and Bonte et al. (1987)



for the  $\mu\text{m}$  sized nuggets, similar depletions of PPGE are observed when compared with chondritic elemental ratios, while Pd which is the most volatile PGE, is almost absent in both these investigations. We plotted all our data on the  $\mu\text{m}$  sized nuggets (Figs. 6 and 7), a sharp trend with respect to depletion of platinum with increasing iridium in the  $\mu\text{m}$  sized nuggets is observed, and strong depletion of Pt, Rh, Pd and also Ru are observed invariably in all the  $\mu\text{m}$  sized nuggets investigated so far.

#### *Nanometer sized nuggets*

In the case of the nanometer sized nuggets, enrichment trends are exactly the opposite of that observed in  $\mu\text{m}$  sized nuggets (Fig. 7). We analysed two hundred and thirteen PGNs in the nanometer sizes in magnetite and wustite phases of the spherules: none of them shows all six Pt-group elements. Further, the refractory Pt-group elements (Os, Ir and Ru) are either totally absent or present in only small percentages in all these nuggets (see Table 4 and Appendix 1). The nanometer nuggets ubiquitously contain platinum, and smaller quantities of Rh. A few rare nuggets also have small percentages of Os and Ir, and Pd as well but these are close to the detection limits of the analytical system. There appears to be proportionality between increasing nugget size and Pt-content (Fig. 8A), and after a critical size is reached Rh appears in detectable quantities in these nuggets, while in some nuggets Ru is also present. Where Rh is present, Pt/Rh in these nuggets is closer to the chondritic ratio of 7.10 (Fig. 10), this points towards a derivation from an unfractionated chondritic parent body, therefore the nanometer nuggets show some level of equilibration as far as the volatile PGEs are concerned and are not completely 'disequilibrated' as suggested by Bonte et al. (1987). The larger nanometer nuggets contain all three volatile Pt-group elements or at least two of them, some of them do show small percentages of the more refractory PGE (See appendix 1) The weight percent of platinum varies between  $< 1 - 20\%$  (Appendix 1) and, with increasing platinum content in these nuggets Fe seems to be decreasing as can be seen in Fig. 8B. They also show a positive trend of Pt with Ni (Fig. 8C), and stronger trend of increasing Rh contents with an increase in the Pt contents (Fig. 8D).

In two spherules (AAS-26-D1-P8 and AAS-22-D3-P3) we observed one  $\mu\text{m}$  sized and several nanometer nuggets in the same cross section. The larger  $\mu\text{m}$  sized nugget contains Os and Ir in chondritic proportions (Table 5), in addition there is a depletion of Rh, Ru and Pt, whereas Pd is completely absent. Whereas, the nanometer nuggets in the same cross contain only Pt (Range: 2.4 - 7.5 %), Rh (0.3 - 0.6 %) and Ru (up to 0.2 %); the more refractory Pt-group elements are absent. All the nanometer nuggets in these spherules are seen only in the magnetite grains. We are looking at

only at one cross-section, obviously, there should be several more such nuggets within the unexposed magnetite grains of the spherules. The volatile PGE depletions shown by the  $\mu\text{m}$  sized nuggets are therefore not real. And by extension, the spherules have not lost the volatile PGEs except perhaps for Pd. Therefore, within the spherule a fractionation and separation of the volatile PGE (Pt, Rh, Pd) from the refractory PGE (Os, Ir, Ru) is observed (Figs. 6 and 7).

Brownlee et al. (1984) reported that the weight percent of platinum could go up to 30 % in  $\mu\text{m}$  sized nuggets. Bonte et al. (1987) reported Pt content up to 44.8 % in the nanometer nuggets observed in I-type spherules and Pt percentages of 38.4, 25.6 and 2.7 %, respectively, in the nuggets found in the lone S-type spherule. It is discernible that the total Pt contained in the nanometer nuggets when added to the larger PGNs in the same spherule would easily lead to a chondritic elemental ratios of PGE. However, Pd is almost absent in both types of nuggets as reported by Brownlee et al. (1984) as well as Bonte et al. (1987). Apparently, it has been volatilized. In the one nanometer nugget where Pd has been reported by Bonte et al. (1987), the Pt/Pd ratio is 3.04 which is much more than the chondritic ratio of 1.70 (Tagle and Berlin 2008), therefore large percentages of Pd appear to have been volatilized even in this nugget. Further, Bonte et al. (1987) observed that the three nanometer nuggets found in the S-type spherule had differing compositions ranging from: Ir-enriched and volatile PGE depleted, volatile PGE-enriched and depleted in refractory PGE, and the third nugget which was intermediate between these two compositions. They suggested that an average composition of these nuggets would add up to be chondritic. The PGE segregation in the lone barred olivine S-type spherule by Bonte et al. (1987) does not appear to follow any fractionation pattern.

#### *Nuggets in Wustite*

Wustite grains have garlands of small shiny nuggets which are Ni-rich. Some of these nugget chains are open ended, these types of chains contain increasing quantities of Ni in a continuous sequence from nugget to nugget. Further, while the Ni content increases along this chain, we also observe appearance of Pt (Figs. 2C and 5) starting from the detection limit of the analytical system and the next few nuggets along the chain contain increasing percentages of Pt.

It is further observed, when such chains are seen in the wustite (or magnetite) portions of the I-type spherules, their Pt-contents are low ( $< 1$  %) and not many discrete nanometer nuggets are observed in the magnetites of these spherules. Also, only Pt is observed in these nuggets in detectable quantities and no other PGE is seen. Whereas, in the spherules where large numbers of nanometer nuggets are observed in the magnetite grains (36 nuggets in AAS-26-D2#1-P2, and 104

nuggets in AAS-26-D1-#2-P1: Fig. 2A), one does not see many nuggets in wustites, and the nugget chains are absent. Here, the Pt contents are much higher (maximum Pt ~ 24 %) and detectable quantities of Rh are common, and rarely other PGE such as Pd, Os and Ir are also observed (see also Table 2 and Appendix 1). Therefore, in the latter types of spherules where large numbers of discrete nuggets are observed in the magnetite portions, segregation of PGE appears to be in a much more advanced state.

In order to explain the nugget formation phenomena, one needs to explain both the nugget types: the large  $\mu\text{m}$  sized ones which contain refractory PGE, the smaller nanometer sized nuggets in magnetite which contain appreciable quantities of Pt, and the nugget chains in wustite which have detectable levels of Pt. Apparently, at some stage of nugget formation, the more volatile PGEs are separating from the refractory Os, and Ir.

## DISCUSSION

### Parent bodies of nugget bearing micrometeorites

Identifying the parent bodies will be a major step forward in the understanding of the micrometeorites as it enables genetic connections. To understand this we plotted the range of Os/Ir (normalized to CI) for different chondrites (CI, CO, CV, CM, CK, CR, CH, CB, K, R, H, L, LL, L/LL, EH, EL) and iron meteorites (IAB, IIAB, IIIAB, IVB) along with  $\mu\text{m}$  sized PGNs from previous work and from this study as shown in Fig. 9. It can be seen that all the chondrites have similar values and fall in a narrow band. The vertical dashed line is the CI line. Iron meteorites of different types have diverse values. The data from seven nuggets seems to fall near the horizontal line of the chondrite value. Other nuggets show a spread and indicate a possibility that they may have originated from iron meteorites, assuming that there was no fractionation during their formation.

In order to estimate the probable dimensions of the parent bodies, we have extrapolated the total concentration of the Os and Ir contained in the  $\mu\text{m}$  sized nuggets in this study to that in a chondritic parent body. Os and Ir are considered because of their refractory nature and also it is assumed that they have suffered the least vaporization among the PGE. Further, we also assume that the nugget which is visible has segregated most of the PGE contained in the parent body efficiently. However, it is important to keep in view that the estimates are for a minimum size of the parent body. The  $\mu\text{m}$  sized nuggets have sizes ranging from 3.6 to 4.9  $\mu\text{m}$ , hosted by spherules having a diameter range of 180 to 300  $\mu\text{m}$ . The calculation indicates that concentration of Os (5.3 to 16.1  $\mu\text{g/g}$ ) and Ir (6.0 to 11.1  $\mu\text{g/g}$ ) are very high when compared with their concentration in chondritic

parent bodies, i.e., 0.4 to 3.5  $\mu\text{g/g}$  (Tagle and Berlin, 2008). Therefore, the parent body of the nugget-bearing spherules if it were chondritic then it should have been of much larger dimensions (at least eight times) than the diameter of the host I-type spherule. Without accurate information on the mass loss during atmospheric entry, it would be difficult to pin point the parent body. Iron meteorites have larger concentrations of Os and Ir contents compared to chondritic meteorites. The concentration of Os and Ir in some of the  $\mu\text{m}$  sized PGNs comfortably falls within the range of iron meteorites thus giving rise to the possibility of an iron meteorite parent body (e.g., see Fig. 9). Brownlee et al. (1984) also pointed out that one of the nuggets observed by them has a Pt/Ir ratio higher than that of chondritic and they did not rule the possibility of a IIIA, B iron meteorite as a parent body. However, the Os/Ir ratios in iron meteorites have a very wide range (Pernicka and Wasson 1987, Campbell and Humayun, 2005), and a majority of the Os/Ir ratios of all the  $\mu\text{m}$  sized nuggets known so far fall close to chondritic ratios (Fig. 9). A majority of the  $\mu\text{m}$  sized nuggets in the present as well as in earlier studies (Brownlee et al. 1984; Bonte et al. 1987) show fractionation patterns that indicate a chondritic parent body. Both these investigating groups suggested small meteoritic metal particles as progenitors. Bonte et al. (1987) further considering the fractionation patterns of Ir, Fe, Ni, Co and Sc suggested a Fe-rich parent body with a minor fraction of chondritic material. More recent investigations by Herzog et al. (1999) detected cosmogenic radionuclides in I-type spherules (I-type spherules host all the nuggets observed in the present study) which implied that these spherules have entered the Earth as primary bodies. Further, based on their stable isotope ratios (Cr/Fe and Fe/Ni) they suggested that the parent bodies of the I-type spherules could be the metal grains in carbonaceous-chondrite-like objects such as CO, CV, and CR chondrites or unequilibrated ordinary chondrites. They ruled out iron meteorites as possible parent bodies of I-type spherules. In view of all the evidence that is available, it appears most likely that the I-type spherules that host nuggets appear to be meteoritic metal from chondritic parent bodies.

### **Nugget formation process**

About 8 % of the I-type spherules examined by us show nuggets of either or both types, therefore the formation of nuggets appears to be fairly common. As suggested by Brownlee et al. (1984) and by virtue of the elemental ratios of the more refractory PGE nuggets in this study, the nugget-bearing spherules show a strong inclination towards a parent body of chondritic composition. Considering a chondritic parent body, especially a carbonaceous chondrite, metal segregation during the initial stages of atmospheric entry takes place by reduction of silicates due to pyrolysis because of burning of carbon in the parent body under low oxygen fugacity (Brownlee et al. 1984). Wustite

subsequently forms under low oxygen fugacity in the upper atmosphere. The spherules upon further heating and oxidation develop a Fe-Ni bead (Brownlee 1985). With the process of oxidation and heating continuing, the noble metals which are surrounded by an immiscible envelope of oxidized material start accumulating into discrete beads of elements more noble than Ni (Brownlee et al. 1984). This process of formation of PGNs has been supported by Bonte et al. (1987) especially for the nuggets found in I-type spherules. However, they did not have a mechanism for the formation of nanometer “disequilibrated” family of nuggets. But they did suggest that the presence the nanometer nuggets comprising volatile PGE indicates that a single process is insufficient to explain both these types of nuggets.

The differences in PGE composition shown by the spherules which contain large numbers of discrete nanometer nuggets in the magnetites and the spherules that contain nugget chains, could provide a clue for PGE segregation and fractionation.

In the spherules where nugget chains are observed, there are very few discrete nanometer nuggets. The discrete nuggets which are mostly found in magnetites, contain high percentages of Pt (up to 24 %), and the presence of Rh and other PGE are also observed in these nuggets (Appendix 1). Whereas the nugget chains are Ni-rich, with some of them containing only Pt, that too in very low percentages (close to the detection limit of the analytical system used). In the spherules where the nugget chains are observed, there are otherwise very few discrete nanometer nuggets in the magnetites. In contrast to the spherules, where large numbers of discrete nuggets are observed in the magnetites (e.g., 104 nanometer sized nuggets in AAS-26-D1-#2-P1), nugget chains are absent (Fig 2A). Therefore, the formation of larger numbers of discrete nuggets in the spherules is an indication that the segregation of the PGE and its fractionation are in an advanced stage in these spherules.

Initial removal of PGE for nugget formation involves platinum, i.e., while palladium gets volatilized during this process due to its non-refractory nature, platinum is the first element that gets separated, isolated amongst the PGE to form discrete nuggets, Ni helps in this process. Pt verses Ni show a positive correlation amongst the nanometer nuggets (Fig. 8C). Pt and Rh have a face centered cubic structure and are more compatible with Ni (which also has a similar structure) as compared with the other PGE (Palme and Wlotzka 1976). Further, the condensation temperatures of Pt and Rh are closest to that of Fe and Ni (Palme 2008). Palme (2008) further suggested that the final stage of PGE extraction will include only Fe-Ni metal extraction. Therefore, Pt and Rh are the two elements that appear to be the first among the PGE to be segregated. This selective uptake of Pt and Rh by Fe-Ni seems to result in the fractionation of the PGE, where the other remaining PGE (i.e., Os, Ir and

Ru) form a large,  $\mu\text{m}$  sized nugget with increasing heating and oxidation. The initial stage in this process seems to be the formation of nugget chains. This is followed by the formation of discrete nanometer nuggets with high Pt and Rh contents. With increased heating and oxidation experienced by the spherule, Os and Ir (which have much higher condensation temperatures than Pt and Rh) appear to segregate and form into a discrete large ( $\mu\text{m}$  sized) nugget. This sequence is discernible from the spherules which display the various stages as described above.

Considering that the entire process is expected to take place in about 5 seconds during atmospheric entry (Brownlee et al. 1984), it would be an extremely efficient process of noble element segregation and fractionation.

The timing of nugget formation if narrowed down, could also throw important light on metal segregation and fractionation of PGE in natural systems. By all accounts, carbothermic processes played a major role in the initial stages of metal segregation during the entry of an unfractionated chondritic body, leading to siderophile depletion in the silicate spherules (Brownlee et al. 1983; Genge and Grady 1998). Formation of two phases: metal and silicate takes place during this process, since the metal phase has by far the larger specific gravity inertial forces would lead to the separation of metal and silicate phases into two different spherules – the I-type and the S-type observed commonly (Blanchard et al. 1980). The CI or CM chondrites (which are the most accepted parent bodies of most micrometeorites – Brownlee et al. 1997; Taylor et al. 2000) contain appreciable quantities of sulphur (~5%). Sulphur-rich phases have extremely high partition coefficients ( $D = >10^4$ ) for PGE between a metal-silicate system (Lorand et al. 2008). Apparently, sulphur has been volatilised even before the I-type spherule could be formed. This is evident because, sulphur-rich phases have been observed in S-type spherules in the form of troilite, pentlandite etc. whereas these are conspicuously absent in the I-type spherules. Retention of sufficient quantities of PGE in the nuggets suggests that the fractionation between the IPGE (iridium-PGE: Ir, Os and Ru) and PPGE (palladium-PGE: Pt, Rh, Pd) took place after the formation of the I-type sphere. The fractionation is apparently taking place in the order of decreasing melting point: Os, Ir, Ru, Pt, Rh, and Pd. In all probability the boiling-point controlled mechanism could probably be responsible. Oxygen fugacity and presence of Ni seem to play a major role in this process. One possible condition that stands out is that of oxygen fugacity, because  $f\text{O}_2$  has greater control than temperature in PGE solubilities, and PGE nuggets have been observed in many experiments conducted under low oxygen partial pressures (Capobianco and Drake 1990; Borisov and Palme 1997).

## **Implications of nugget formation**

There are several implications to this phenomenon of nugget formation and fractionation of PGE.

### *Understanding mantle differentiation processes*

Although, PGE were considered geochemically coherent and strongly siderophile earlier, increasing number of studies over the last several decades have pointed to both concentration and fractionation of PGEs in planetary processes (Fleet and Stone 1991). During the partial melting of the mantle, the PGEs are fractionated into two groups (Capobianco and Drake 1990):

- a) IPGEs or the iridium-PGEs: These are considered compatible in igneous systems. Mantle rocks such as the peridotites are enriched in these elements.
- b) PPGEs or the Palladium-PGEs: These comprise of Pt, Rh and Pd which are considered incompatible in igneous processes. Mantle-derived magmas (e.g., MORBs) are relatively enriched in PPGEs (Lorand et al. 2008).

During planetary core formation, the PGE are strongly partitioned into Fe-Ni metal and are to a great extent removed from the mantle. However, the near chondritic abundance patterns of the PGE in the mantle (although depleted in concentration by several orders of magnitude) has been attributed to a late addition of chondritic material by repeated bombarding of the Earth after its core formation – this is the well known “late veneer” model (Chou 1978). However, the fractionated chondrite normalized patterns shown by PGE among residual mantle rocks and mantle derived magmas has puzzled investigators for decades.

PGE abundances in magmas such as MORBs produce positively sloped patterns, whereas mantle rocks such as lherzolites, peridotites show a negatively sloped patterns of PGE when plotted in the order of decreasing melting temperature (Os>Ir>Ru>Pt>Rh>Pd) (Lorand et al. 2008). Olivine and chrome-spinel have been identified as the two minerals which could sequester the PGE, where olivine crystal structure accommodates Os and Ir (Brenan et al. 2005), and Cr-spinel can accommodate Ir, Ru and Rh (Capobianco and Drake 1990; Righter et al. 2004). This explanation although plausible, cannot account for the total budget of PGE in the mantle. In addition, this process is further complicated by the formation of PGE-rich micronuggets under low  $fO_2$ , especially in the case of Cr spinel ( Borisov and Palme 1997; Capobianco and Drake 1990), which leads to

inhomogeneous distribution of Pt as shown by experiments at low oxygen fugacity by these investigators.

In all the investigations, it has been observed that the presence of sulphur plays a key role in view of the known affinity of PGE for sulphides and also extremely high partition coefficient of PGE between metals and silicate materials ( $D^{\text{metal/silicate}} = >10^4$ , Lorand et al. 2008). The PGE in the Earth have been sequestered by phases containing sulphur albeit in a different mineralogical and geochemical compositions. Further, the volatile depletion in planetary materials of all the four known sources (i.e., Earth, Moon, Mars, and Vesta) suggests that after the separation of sulphur-rich metals, Fe-Ni metal will dominate in the sequestering of PGE (Palme 2008).

This is found to be true in the present case. Because, once an I-type spherule forms, sulphur minerals are generally not seen, only a Fe-Ni spherule with a combination of wustite and magnetite in varying percentages. Therefore extremely efficient fractionation of the PGE into Os-Ir-Ru and Pt-Rh sub-groups takes place in a melt that has only Fe-Ni, dominantly Fe and less Ni because substantial percentage of Ni has been removed in the form of a Fe-Ni bead. Borisov and Palme (1997) predicted the occurrence of Pt-Fe alloys in terrestrial magmas for fractionating Pt from other noble metals. It is seen from the data here, that a majority of the fractionation appears to take place in the system where only Fe-Ni is present where heat and oxidation seem to play a major role. The high resistance of PGE to oxidation leads to extremely efficient extraction with metallic Fe-Ni during metal segregation and core formation (Palme 2008). Because of this property, major proportions of the highly siderophile elements have long migrated to the Earth's core. The observations presented here indicate that PGE fractionates in a Fe-Ni system, therefore, the data presented here also points towards planetary cores which could probably have fractionated PGEs.

#### *PGE analysis in impact cratering phenomena*

Meteorites are highly enriched in the platinum-group elements (PGE), because of which and also in view of their refractory nature, the analysis of PGE contents in meteorite impact ejecta has been used commonly for identification of the impacting projectile, and also for estimating the size of the impacting bolide (Morgan et al. 1975; Evans et al. 1993; Tagle and Claeys 2005; Tagle and Hecht 2006; Tagle and Berlin 2008). Impact spherules have been found in several horizons in the form of microkrystites (Czajkowski 1987; Kyte et al. 1992; Glikson 2004; Glikson and Allen 2004; Glikson 2005). Glikson (2006, 2007) observed fractionated siderophile and PGE element patterns in the impact spherules of the Archaean Barberton greenstone belt of South Africa and also in the impact ejecta of Pilbara and Kaapvaal cratons in Australia. Sharp differences have been observed



between the refractory (Os, Ir, Ru) and volatile (Pt, Rh, Pd) PGE contents of these impact ejecta. The ejecta also showed signals of low-oxygen fugacities in the Archaean atmosphere in the form of low  $\text{Fe}_2\text{O}_3/\text{FeO}$  ratios, especially when compared with similar spherules found at the K/T boundary (Byerly and Lowe 1994). Selective enrichment in the refractory PGE relative to volatile PGE has been found consistently, especially among the impact basins of the Archaean age (Kyte et al. 1992; Glikson 2004; Glikson and Allen, 2004; Glikson 2005). Therefore, oxygen fugacity appears to be an influencing factor in the fractionation of PGE. Further, this process of PGE fractionation in terms of preferential atmospheric condensation has been attributed to “boiling point-controlled differential condensation from the vapour cloud” (Glikson 2007).

Further, analysis of the presence of PGE-rich micronuggets with high levels of refractory PGE and volatile PGE depleted patterns which were found to be near-chondritic to volatile depleted, which is similar in character to the patterns shown by Brownlee et al. (1984) for the  $\mu\text{m}$  sized nuggets observed in I-type cosmic spherules. The process of formation of these micronuggets in Archaean impact ejecta as suggested by Glikson (2007), is similar to that experienced by the PGNs in cosmic spherules (Brownlee et al. 1984) i.e., as the vaporized material in the ejecta plume moves upwards from a low oxygen, vacuum environment subsequent to an impact, it gets oxidized leading to segregation and enrichment of the unoxidisable more noble elements as nuggets. Byerly and Lowe (1994) made a more direct comparison of this phenomenon with the process undergone by micrometeorites during their atmospheric entry –they suggested the formation of impact spherules in terms of condensation from a mixture of bolide and target which had undergone modification during re-entry.

Brownlee et al. (1984) made an important observation that the first occurrence of nuggets in geologic horizons on the Earth would be indicative of the total oxygen content in the Earth’s atmosphere. This concept has been substantiated qualitatively by the PGE abundance patterns shown by Glikson (2007), Kyte et al. (1992) and others, which are indicative of low oxygen fugacity characteristic of the early Earth’s atmosphere during the Archaean times. The fractionated PGE patterns seen in the spherules in the present study and in the Archaean impact spherules further substantiate the prediction made by Brownlee et al. (1984).

### *Meteoritic Metals in the tropopause*

A large fraction of the micrometeorites entering Earth are completely vaporized in the atmosphere yielding nanometer sized material called meteoric smoke particles ( Hunten 1980; Turco 1982; Gabrielli et al. 2004). This evaporated micrometeoritic material is observable by sensitive

radars (Janches et al. 2009). From the present study, it appears that large numbers of PGNs are released during the atmospheric entry of micrometeorites, because phenomenon of nugget formation is found to be reasonably common (8% of the I-type spherules in this collection have nuggets). Therefore the nuggets released in the atmosphere, could possibly also form a part of meteoric smoke particles, which have not been physically captured so far (Rietmeijer 2000).

## CONCLUSIONS

Polished sections of 175 I-type spherules recovered from the sediments of Indian Ocean by magnetic methods reveal platinum group nuggets (PGNs) in 13 spherules and nugget formation during atmospheric entry appears to be fairly common in I-type spherules. Two types of nuggets differing in size and chemical composition are observed in these spherules. The larger  $\mu\text{m}$  sized nuggets (largest 4.9  $\mu\text{m}$  diameter) contain dominantly refractory PGE i.e., Os, Ir, and Ru whereas the smaller nanometer sized nuggets contain only the volatile PGE i.e., Pt, Rh and Pd. The micrometer sized nuggets are observed only in magnetites and are mostly located at the edge of the spherules, whereas the nanometer sized nuggets are disseminated throughout the spherules and occur predominantly in magnetite grains but sometimes in the wustite grains also. The elemental ratios of the PGE in both these nugget types suggest a chondritic parent body. Both the types of nuggets are found to occur in the same spherule which implies that the PGEs are being fractionated during atmospheric entry into the above two sub-groups due to heating, and oxidation during atmospheric entry. Alternatively, such PGE fractionation is a primary phenomenon which took place in the parent body itself, because the presence of  $^{26}\text{Al}$  and  $^{10}\text{Be}$  in I-type spherules gives rise to the possibility that some of them may not be a product of atmospheric ablation but could be of primary origin (Herzog et al. 1999). Either way, this is the first time that distinct, fractionated PGE patterns have been found to co-exist in a single (very small) object. This phenomenon has implications in three different areas: (1) Fractionation of the PGE has so far been most commonly observed among mantle rocks and mantle derived magmas – but in both these materials sulphur-rich minerals with differing geochemical behaviour have been responsible for sequestering and fractionating the PGE. The observations presented here indicate that PGE also fractionates efficiently in a Fe-Ni system, therefore, the data presented here also points towards a process which could lead to the phenomenon where planetary cores could probably have fractionated PGEs. (2) PGE nuggets found in Archaean impact spherules show fractionated signatures. Such fractionation has been attributed to processes that are similar to those responsible for formation of PGE nuggets in the micrometeorites during atmospheric entry. Therefore, the similarities in both these processes which results in fractionated PGEs substantiates earlier observations of Brownlee et al. (1984) regarding the scope for

understanding processes in the ancient Earth. (3) It appears that the Earth receives a large flux of nanometer nuggets in view of the hundreds of them generated during atmospheric entry of micrometeoroids.

### ACKNOWLEDGEMENTS

We are grateful to the Director, National Institute of Oceanography (NIO) for providing the facilities and the encouragement for this work. We are indebted to G.F. Herzog for the incisive comments and suggestions which helped improve the manuscript substantially. We are also grateful to D.E. Brownlee for the editorial handling and invaluable suggestions for improving the manuscript. The authors are also grateful to Physical Research Laboratory, Ahmedabad, for the sanction of the PLANEX project, under which this work has been carried out. We are grateful to Dipak Panda for the help in EPMA analysis. We are thankful to Vijay Khedekar for the assistance during the SEM-EDS work. This research has made use of NASA's Astrophysics Data System. This is NIO's contribution No. ....

### References

- Blanchard M. B., Brownlee D. E., Bunch T. E., Hodge P. W., Kyte F. T. 1980. Meteoroid ablation spheres from deep-sea sediments. *Earth and Planetary Science Letters* 46:178-190.
- Bonte Ph., Jehanno C., Maurette M., and Brownlee D. E. 1987. Platinum metals and microstructure in magnetic deep sea cosmic spherules. *Journal of Geophysical Research* 92: 641-648.
- Borisov A., and Palme H. 1997. Experimental determination of the solubility of platinum in silicate melts, *Geochimica Cosmochimica Acta* 61: 4349-4357.
- Brenan J. M., McDonough W. F., and Ash R. 2005. An experimental study of the solubility and partitioning of iridium, osmium and gold between olivine and silicate melt. *Earth and Planetary Science Letters* 237: 855-872.
- Brownlee D. E. 1985. Cosmic Dust: Collection and Research. *Annual Review of Earth and Planetary Sciences* 13: 147-173.
- Brownlee D.E., Tomandl D.A., and Olsewski E. 1977. Interplanetary dust: A new source of extraterrestrial material for laboratory studies. *Proceedings of Lunar Science Conference 8<sup>th</sup>*: 149-160.
- Brownlee D. E., Bates B., and Beauchamp R. H. 1983. Meteor ablation spherules as chondrule analogs. *IN: Chondrules and their origin, Houston, TX, Lunar and Planetary Institute*: 10-25.
- Brownlee D. E., Bates B. A., and Wheelock M. M. 1984. Extraterrestrial platinum group nuggets in deep-sea sediments. *Nature* 309: 693-695.
- Brownlee D. E., Bates B., and Schramm L. 1997. The elemental composition of stony cosmic spherules. *Meteoritics Planetary Science* 32: 157-175.

- Brownlee D. E., Blanchard M. B., Cunningham G. C., Beauchamp R. H., and Fruland R. 1975. Criteria for identification of ablation debris from primitive meteoric bodies. *Journal of Geophysical Research* 80: 4917-4924.
- Brownlee D. E., Pilachowski L. B., Hodge P. W. 1979. Meteorite Mining on the Ocean Floor. *Lunar and Planetary Science conference* 10:157-158.
- Bruun A F., Langer E., and Pauly H. 1955. Magnetic particles found by raking the deep-sea bottom. *Deep Sea Research* 2: 230-246
- Byerly G R., and Lowe D R. 1994. Spinel from Archean impact spherules. *Geochimica et Cosmochimica Acta* 58: 3469-3486.
- Campbell A., and Humayun M. 2005. Compositions of group IVB iron meteorites and their parent melt. *Geochimica et Cosmochimica Acta* 69:4733-4744.
- Capobianco C. J., and Drake M. J. 1990. Partitioning of ruthenium, rhodium, and palladium between spinel and silicate melt and implications for platinum group element fractionation trends, *Geochimica et Cosmochimica Acta* 54: 869–874.
- Chou C L. 1978. Fractionation of siderophile elements in the Earth's upper mantle. *Proceedings of the 9th Lunar and Planetary Science Conference*: 219-230.
- Czajkowski J. 1987. Cosmo and geochemistry of the Jurassic hardgrounds. Ph.D. thesis, University of California, San Diego, 418 pp.
- Evans N.J., Gregoire D.C., Grieve R.A.F., Goodfellow W.D., and Veizer J. 1993. Use of platinum-group elements for impactor identification: terrestrial impact craters and Cretaceous–Tertiary boundary. *Geochimica et Cosmochimica Acta* 57: 3737–3748.
- Feng H., Jones K.W., Tomov S., Stewart B., Herzog G.F., Schnabel C., and Brownlee D.E. 2005. Internal structure of type I deep-sea spherules by X-ray computed microtomography. *Meteoritics and Planetary Science* 40:195-206
- Fleet M.E., and Stone W.E. 1991. Partitioning of platinum-group elements in the Fe-Ni-S system and their fractionation in nature. *Geochimica et Cosmochimica Acta* 55: 245-253.
- Gabrielli, P., Barbante C., Plane J. M. C., Varga A., Hong S., Cozzi G., Gaspari V., Planchon, F. A. M., Cairns W., Ferrari C., Crutzen, P., Cescon P., Boutron, C. F. 2004. Meteoric smoke fallout over the Holocene epoch revealed by iridium and platinum in Greenland ice. *Nature* 432: 1011-1014.
- Genge M. J., and Grady M. M. 1998. Melted micrometeorites from Antarctic ice with evidence for the separation of immiscible Fe-Ni-S liquids during entry heating. *Meteorites and Planetary Science* 33: 425 – 434.
- Genge M. J., Engrand C., Gounelle M., and Taylor S. 2008. The classification of micrometeorites. *Meteorites and Planetary Science* 43: 497 – 515.
- Glikson A., and Allen C. 2004. Iridium anomalies and fractionated siderophile element patterns in impact ejecta, Brockman Iron Formation, Hamersley Basin, Western Australia: evidence for a

major asteroid impact in simatic crustal regions of the early Proterozoic Earth. *Earth and Planetary Science Letters* 220: 247-264.

Glikson A.Y. 2004. Early Precambrian asteroid impact-triggered tsunamis: excavated seabed, debris flows, exotic boulders, and turbulence features associated with 3.472 Ga-old asteroid impact fallout units, Pilbara Craton, Western Australia. *Astrobiology* 4: 19–50.

Glikson A.Y. 2005. Asteroid/comet impact clusters, flood basalts and mass extinctions: significance of isotopic age overlaps. *Earth and Planetary Science Letters* 236: 933–937.

Glikson A.Y. 2006. Asteroid impact ejecta units overlain by iron-rich sediments in 3.5–2.4 Ga terrains, Pilbara and Kaapvaal cratons: accidental or cause–effect relationships?. *Earth and Planetary Science Letters* 246: 149–160.

Glikson A.Y. 2007. Siderophile element patterns, PGE nuggets and vapour condensation effects in Ni-rich quench chromite-bearing microkrystite spherules, 3.24 Ga S3 impact unit, Barberton Greenstone Belt, Kaapvaal Craton, South Africa. *Earth and Planetary Science Letters* 253: 1–16.

Herzog G. F., Xue S., Hall G. S., Nyquist L. E., Shih C. -Y., Wiesmann H., and Brownlee D. E. 1999. Isotopic and elemental composition of iron, nickel, and chromium in type I deep-sea spherules: implications for origin and composition of the parent micrometeoroids. *Geochimica et Cosmochimica Acta* 63: 1443–1457.

Hunten D. M. 1980. Rings of Uranus: Proposed Model Is Unworkable. *Science* 208: 625-626

Janches D., Dyrud, L. P., Broadley S. L., and Plane J. M. C. 2009. First observation of micrometeoroid differential ablation in the atmosphere. *Geophysical Research Letters* 36: L06101-06105.

Kyte F.T., Zhou L., and Lowe D.R. 1992. Noble metal abundances in an early Archaean impact deposit. *Geochimica et Cosmochimica Acta* 56: 1365–1372.

Lorand J-P., Luguet A., Alard O. 2008. Platinum-group elements: A new set of key tracers for the Earth's interior. *Elements* 4: 247-252.

Love S. G., and Brownlee D. E. 1993. A Direct Measurement of the Terrestrial Mass Accretion Rate of Cosmic Dust. *Science* 262: 550 – 553.

Maurette M., Hammer C., Brownlee D. E., Reeh N., Thomsen H.H. 1986. Placers of Cosmic Dust in the Blue Ice Lakes of Greenland. *Science* 233: 869-872.

Maurette M., Olinger C., Christophe Michel-Levy M., Kurat G, Pourchet M., Brandstatter F., and Bourot-Denise M. 1991. A collection of diverse micrometeorites recovered from 100 tonnes of Antarctic blue ice. *Nature* 351: 44 – 47.

- Millard H. T., Jr., and Finkelman R. B. 1970. Chemical and mineralogical compositions of cosmic and terrestrial spherules from a marine sediment. *Journal of Geophysical Research* 75: 2125-2134.
- Morgan J.W., Higuchi H., Ganapathy R., and Anders E. 1975. Meteoritic material in four terrestrial meteorite craters. *Proc. Lunar and Planetary Science Conference 6<sup>th</sup>*, 1609-1623.
- Palme H., and Wlotzka F. 1976. A metal particle from a Ca,Al-rich inclusion from the meteorite Allende, and the condensation of refractory siderophile elements. *Earth and Planetary Science Letters* 33: 45-60.
- Palme H. 2008. Platinum-group elements in cosmochemistry. *Elements* 4: 233-238.
- Parashar K., Shyam Prasad M., and Chauhan S.S. 2010. Investigations on a large collection of cosmic dust from the Central Indian Ocean. *Earth, Moon, and Planets* DOI 10.1007/s11038-010-9362-3
- Pernicka E., and Wasson J. T. 1987. Ru, Re, Os, Pt and Au in iron meteorites. *Geochimica et Cosmochimica Acta* 51: 1717–1726.
- Peucker-Ehrenbrink B., and Ravizza G. 2000. The effects of sampling artifacts on cosmic dust flux estimates: a reevaluation of nonvolatile tracers (Os, Ir). *Geochimica et Cosmochimica Acta* 64:1965-1970.
- Pouchou J.L., and Pichoir F. 1991. Quantitative analysis of homogeneous or stratified microvolumes applying the model “PAP”. *Electron Probe Quantitation, Eds. Heinrich & Newbury, Plenum Press N.Y.*, 31-75.
- Rietmeijer F.J.M. 2000. Interrelationships among meteoric metals, meteors, interplanetary dust, micrometeorites, and meteorites. *Meteoritics and Planetary Science* 35: 1025–1041.
- Righter K., Campbell A.J., Humayun M., and Hervig R.L. 2004. Partitioning of Ru, Rh, Pd, Re, Ir, and Au between Cr-bearing spinel, olivine, pyroxene and silicate melts. *Geochimica et Cosmochimica Acta* 68: 867-880.
- Tagle R., and Claeys Ph. 2005. An ordinary chondrite impactor for the Popigai crater, Siberia. *Geochimica et Cosmochimica Acta* 69: 2877–2889.
- Tagle R., and Hecht. L. 2006. Geochemical identification of projectiles in impact rocks. *Meteoritics and Planetary Science* 41:1721–1735.
- Tagle R., and Berlin J. 2008. A database of chondrite analyses including platinum group elements, Ni, Co, Au, and Cr: Implications for the identification of chondritic projectiles. *Meteoritics & Planetary Science* 43: 541-559.
- Taylor S., Lever J., and Harvey R. 2000. Numbers, types and compositional distribution of an unbiased collection of cosmic spherules. *Meteoritics and Planetary Science* 35: 651-666.
- Turco R. P. 1982. Models of stratospheric aerosols and dust. *Chapter 4, Stratospheric Aerosols, R. C. Whitten (Ed.), Springer-Verlag, Heidelberg*, pp. 93-119.

## Figure Captions

### Figure 1

Micrometeorites with  $\mu\text{m}$  sized nuggets.

**A,B:** SEM image of external surface of I-type spherule, AAS-26-D1-Hh with a PGN on within the encircled region. Magnified version of the nugget is shown in B.

**C,D:** Polished section of AAS-26-D1#1-P8 with a  $\mu\text{m}$  sized nugget. The spherule has dominantly magnetite (dark portion) with very less wustite contents (grey portion), along with a magnetite rim. "D" is a magnified version of the nugget. The larger nugget contains dominantly refractory PGE. Several nanometer sized nuggets are also seen in this image which has dominantly Pt and at times smaller percentages of Rh. The PGE appear to be fractionated between the larger  $\mu\text{m}$  sized nuggets (which have higher Ir and Os contents) and the nanometer sized nuggets which have only Pt and Rh among the PGE.

**E,F:** AAS-26-D1#1-P9 which has a dominant magnetite component compared with the grey colored wustite. A  $\mu\text{m}$  sized nugget is clearly seen in the cross-section. However, nanometer nuggets appear to be absent in this view.

**G,H:** AAS-22-D3-P4, I-type spherule which again has a dominant magnetite portion, there are hollow areas within the spherule which could have been generated either due to shrinkage or due to the escape of volatile elements during atmospheric entry.

### Figure 2

A) Nanometer sized nuggets in the cross section of AAS-26-D1-#2- P1. The nuggets are distributed throughout the spherule especially in the magnetite portions. Inset shows one of the nuggets under high magnification.

B) The spherule AAS26-D1-#1- P8 has both the  $\mu\text{m}$  and nanometer sized nuggets.

C) Chain of nanometer sized nuggets in the wustite region of a spherule. Nugget numbers 24, 25, 26 which are at the head of the chain show detectable quantities of platinum. The other nuggets show enhanced quantities of Ni. Number 16 is a nugget in magnetite.

### **Figure 3**

High magnification images of nanometer nuggets in magnetite grains. These types of nuggets are dominantly found in magnetites and contain only Pt and at times low percentages of Rh among the PGE. The larger and brighter nuggets have higher Pt contents, these nuggets also contain Rh.

### **Figure 4**

Nuggets in wustite portion of micrometeorites. PGNs in wustite portions are rare. They have similar diameters as the nuggets observed in magnetites, these are mostly at the edge of magnetites implying that they have migrated from the magnetite portions. These individual nuggets are different from the nugget chains usually observed in wustites as shown in Fig. 5

### **Figure 5**

Chains of nuggets in magnetite and wustite portions of spherules. The brightest nuggets in the chain contain detectable quantities of platinum. The other nuggets in the chain are Ni-rich. The Pt-bearing nuggets are generally one or two such spots which have brightest shine under the backscattered electron image mode of the SEM. The total Pt contents in the nuggets in these chains is much less than the nanometer nuggets that are observed in magnetites.

### **Figure 6**

Ir and CI chondrite normalized PGE composition of the  $\mu\text{m}$  sized nuggets compared with chondritic meteorites (Filled square, open square, Filled circle, open triangle, filled inverted triangle are LL, EL, CI, H and CV, respectively.) The shaded region is of the  $\mu\text{m}$  sized nuggets analysed in this study. Depletion of Pt, Rh, and Pd when compared with chondritic ratios are discernible in this figure.

### **Figure 7**

The PGE data of all  $\mu\text{m}$  and nanometer sized nuggets normalized with CI chondrite. The dashed line represents the average for the  $\mu\text{m}$  sized and nanometer nuggets, respectively. Enrichment of Os and



Ir is observed in the  $\mu\text{m}$  sized nuggets, whereas in the nanometer nuggets Pt and Rh appear to be enriched with respect to CI chondrites.

### **Figure 8**

Elemental correlations in nanometer nuggets.

**A.** Graph of size of nanometer sized nuggets in nm versus Pt concentration in wt%. The Pt content appears to be strongly correlated with nugget diameter.

**B.** Plot showing the Pt content of the nuggets is negatively correlated with Fe.

**C:** Plot showing Ni versus Pt contents of the nuggets. A strong positive correlation is discernible.

**D:** Plot showing Pt versus Rh contents of the nuggets. Weak positive correlation is seen.

### **Figure 9**

The Os/Ir (normalized to CI) nugget data from Brownlee et al. (1984), Bonte et al. (1987) and from the present study along with all chondrites values and few iron meteorites.

### **Figure 10**

Chondrite normalised ratios of the different Pt-group elements for  $\mu\text{m}$  sized larger nuggets. The ratio between different PGE normalized to CI is poor except in the case of Os/Ir.

Figure 1

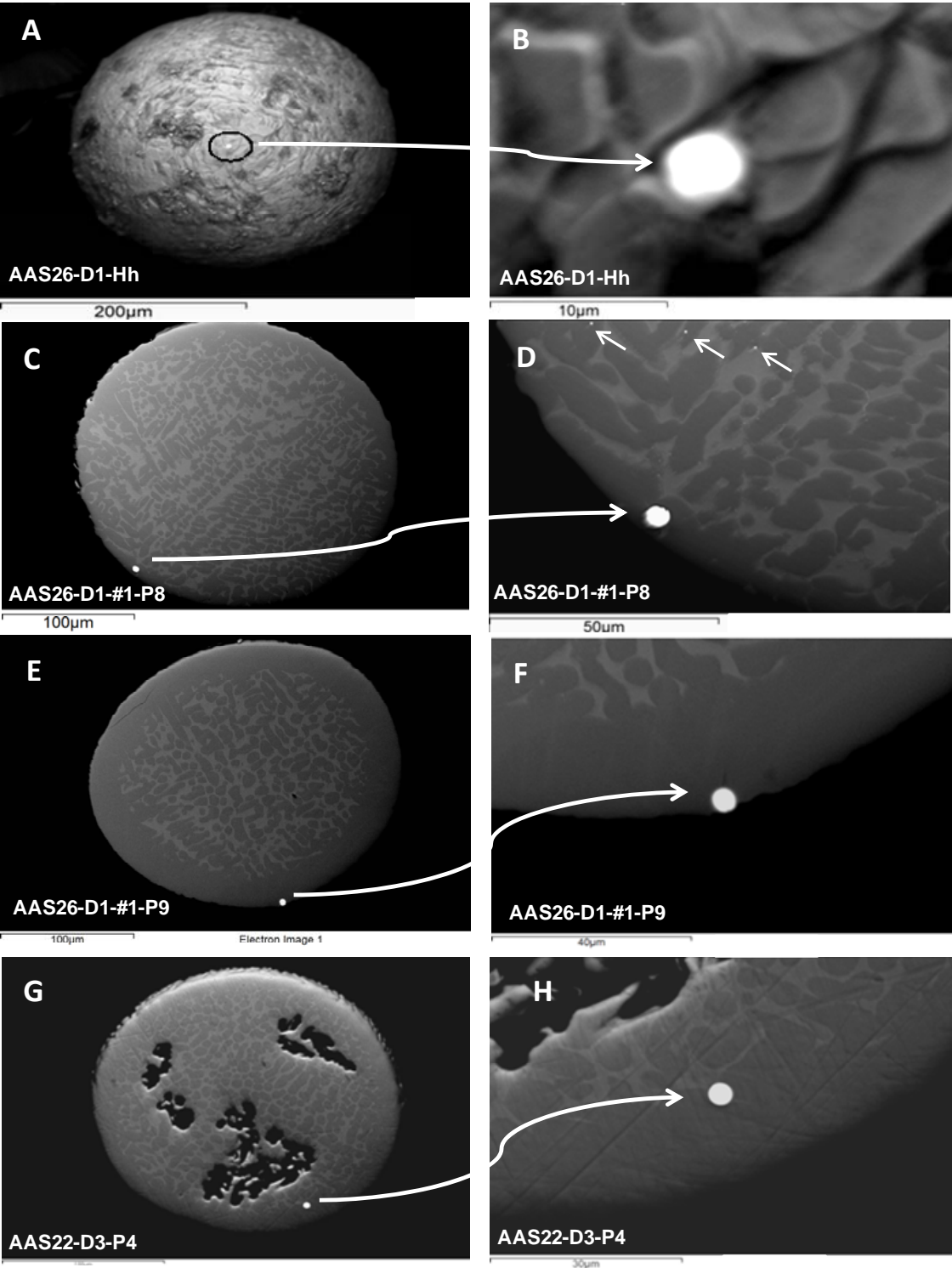


Figure 2

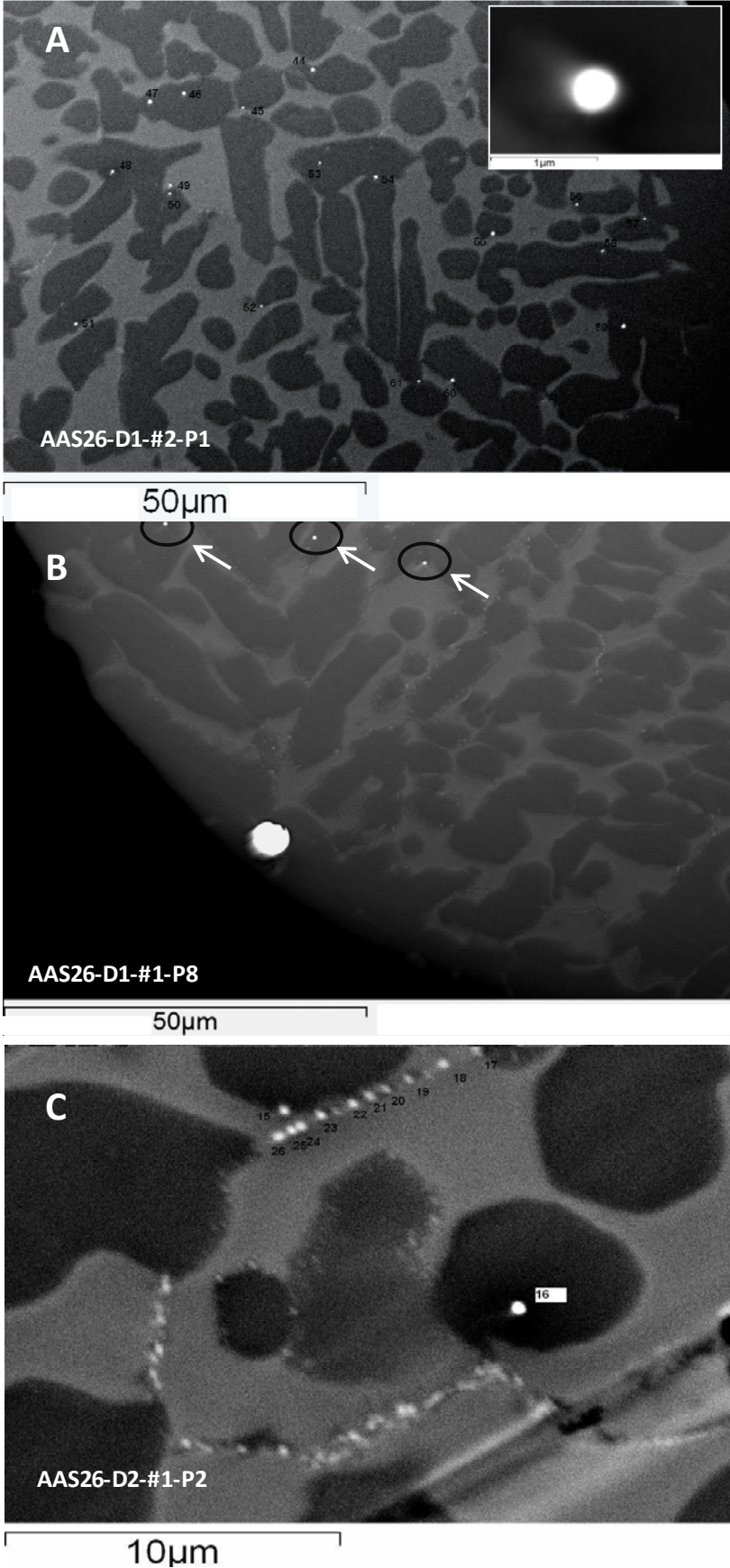


Figure 3

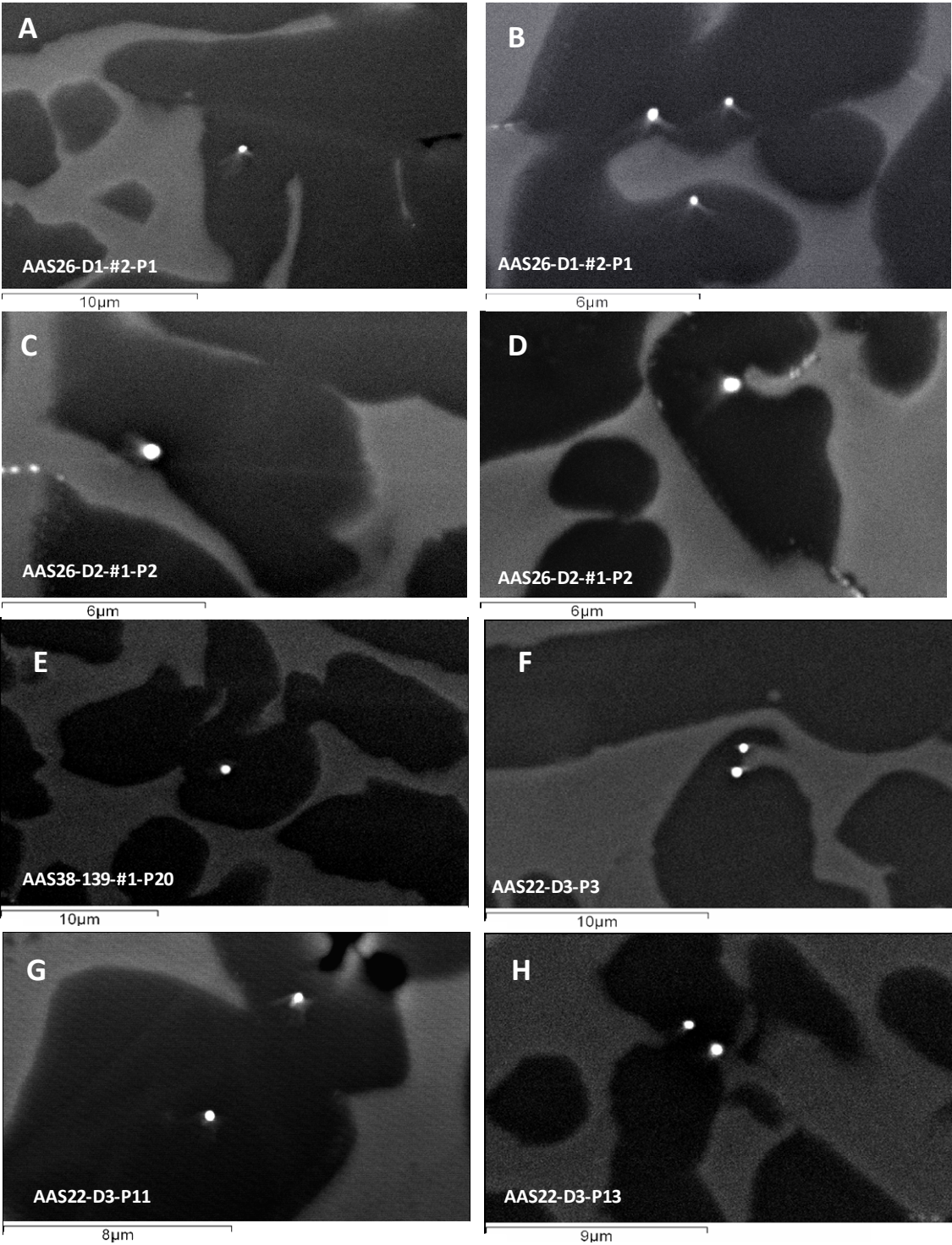


Figure 4

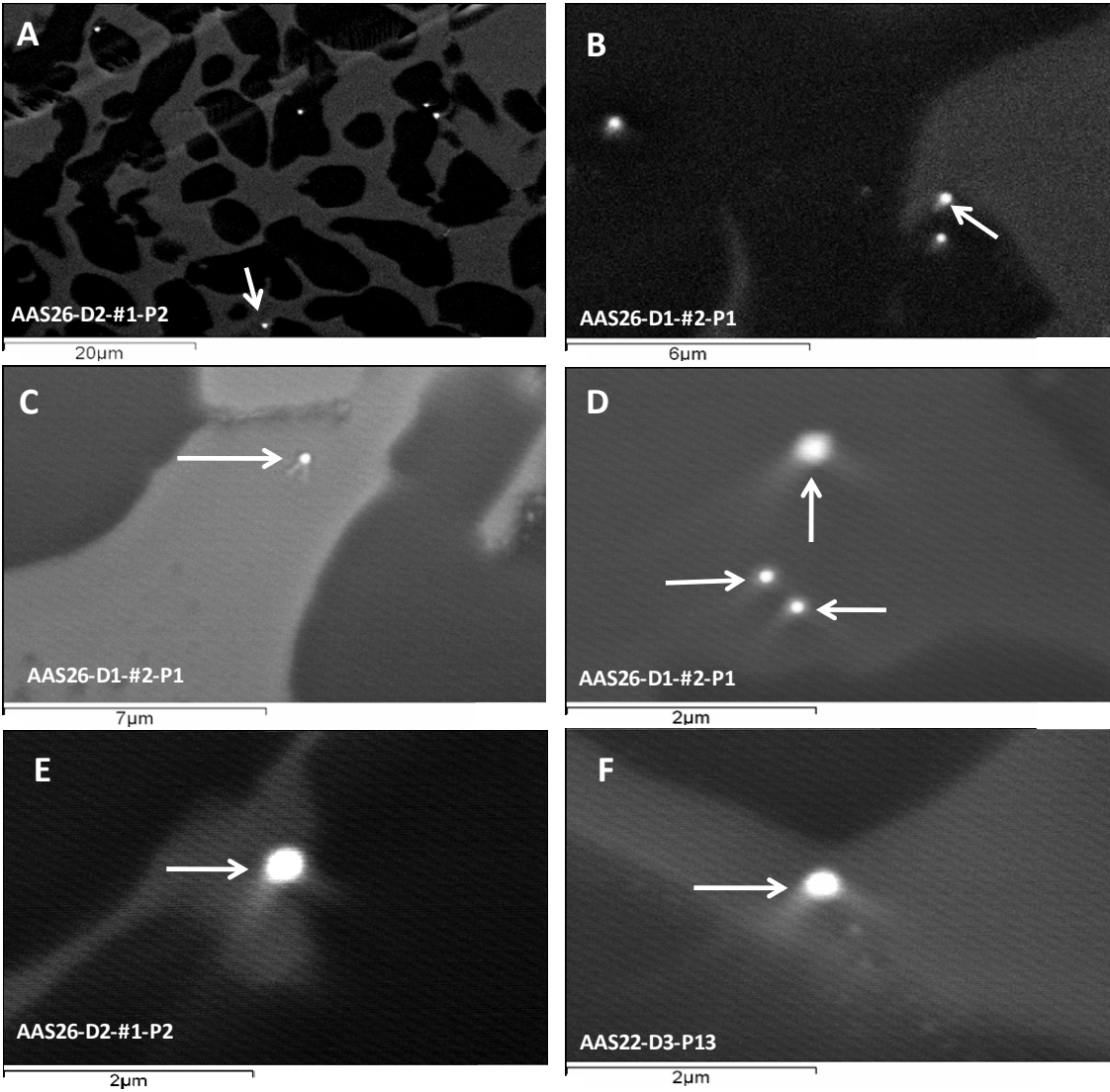


Figure 5

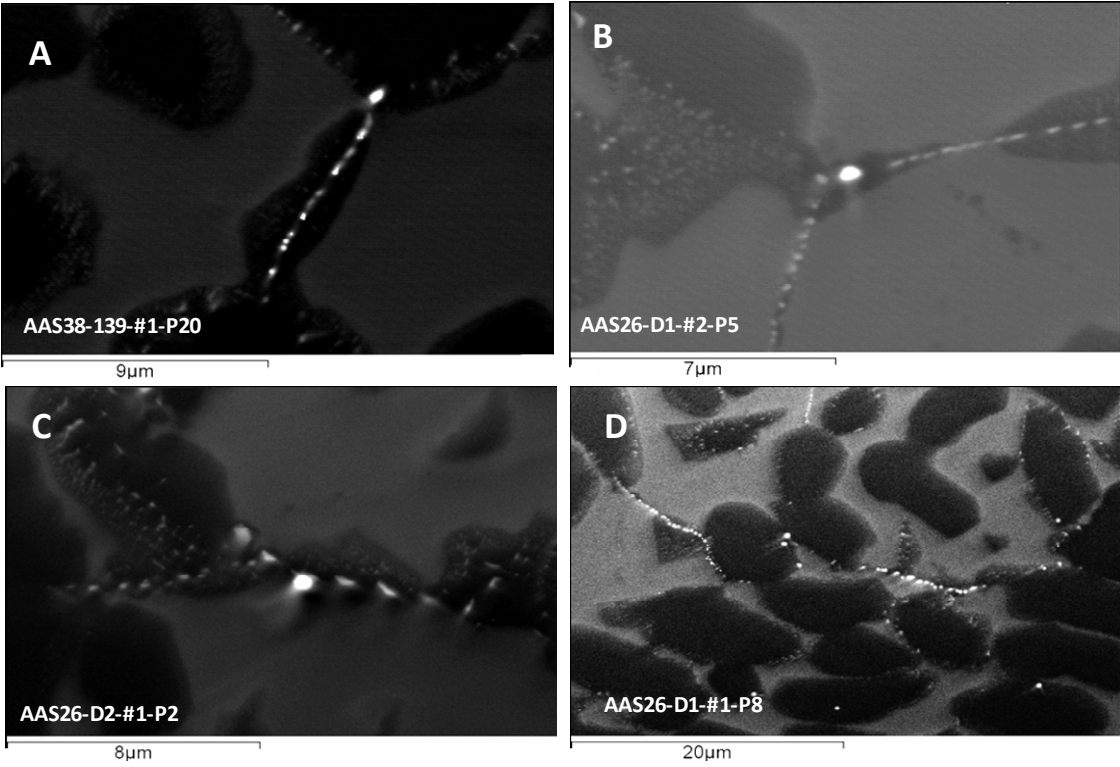


Figure 6

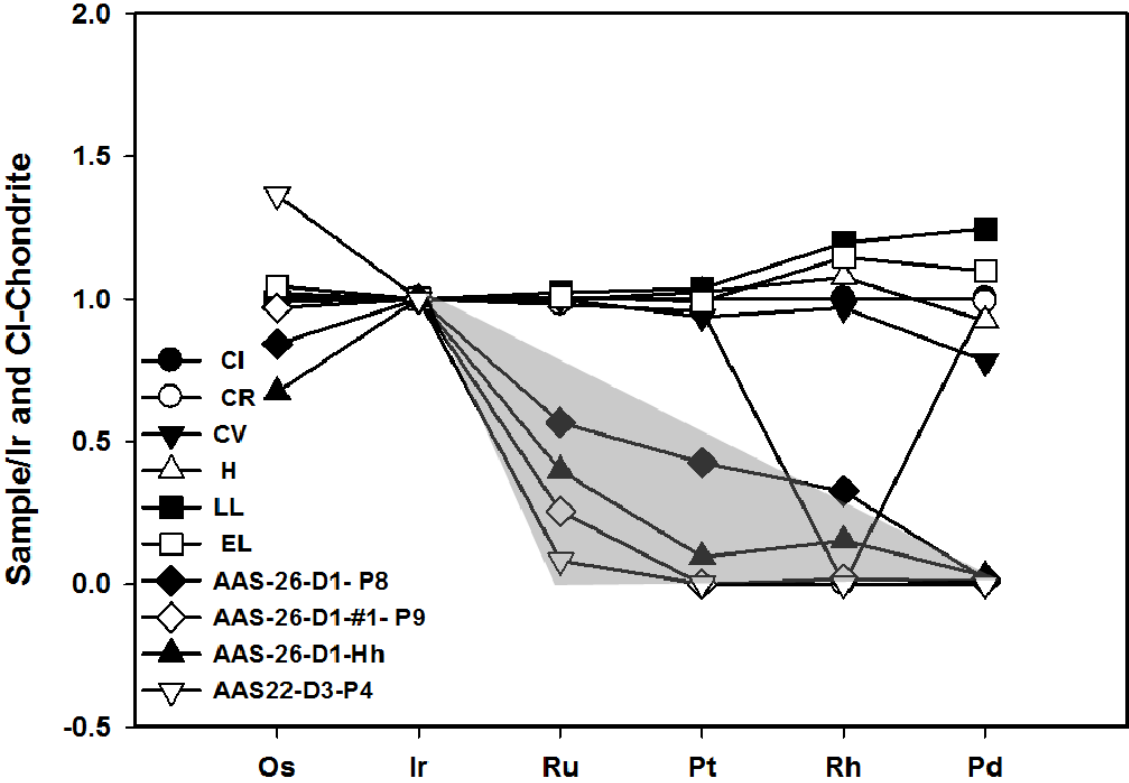


Figure 7

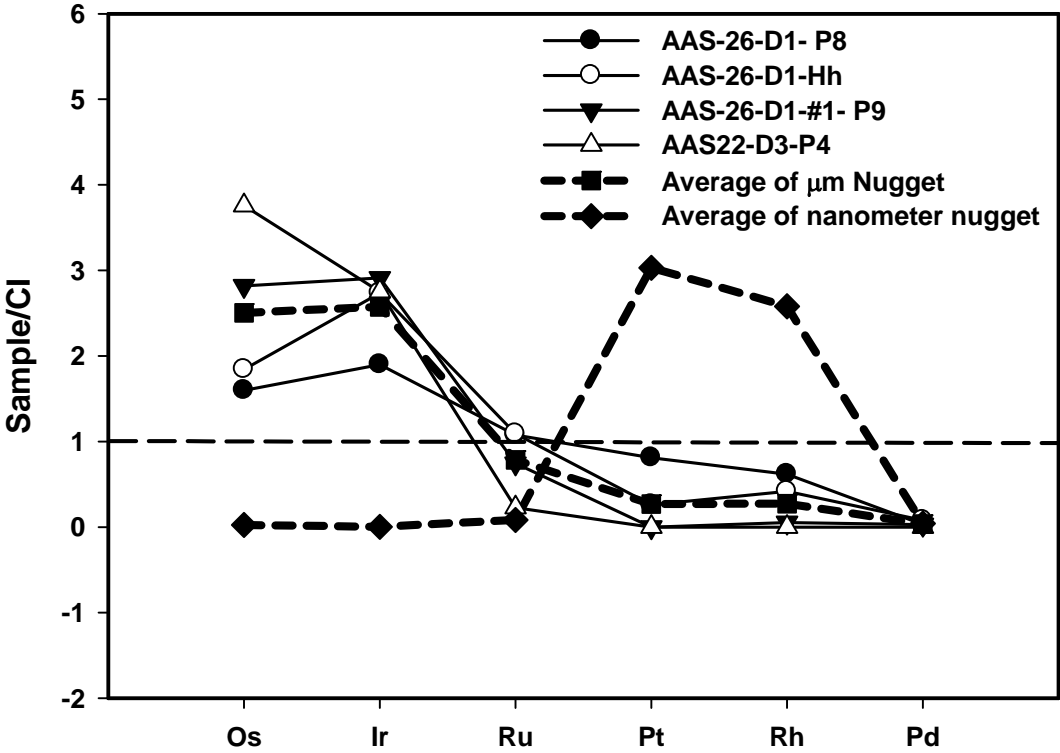




Figure 8

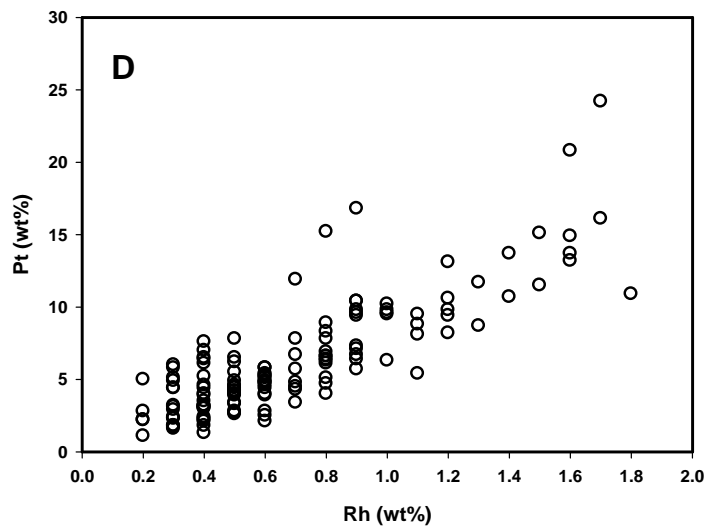
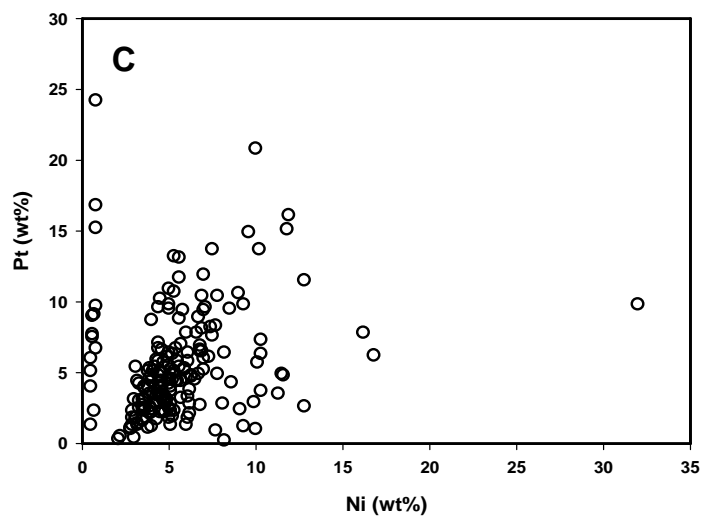
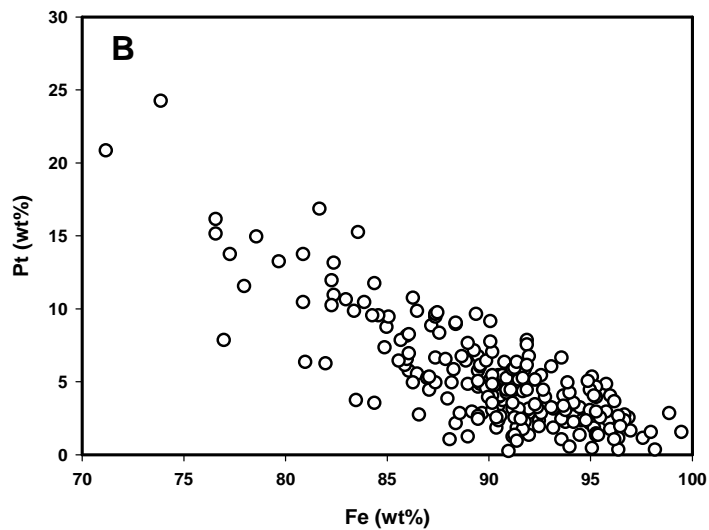
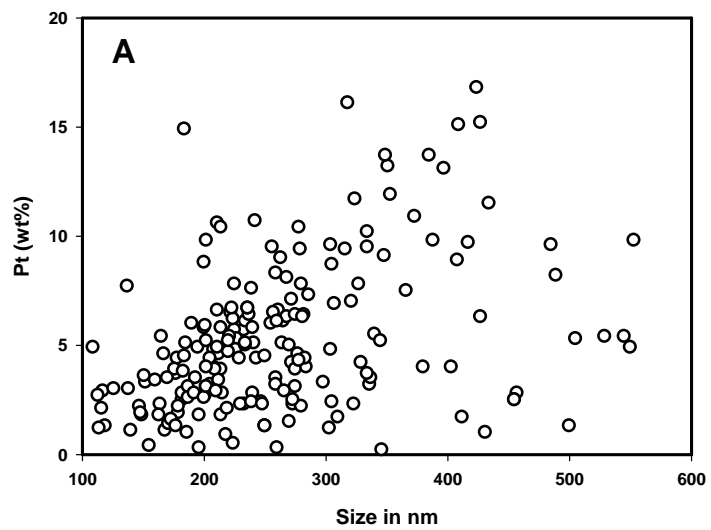


Figure 9

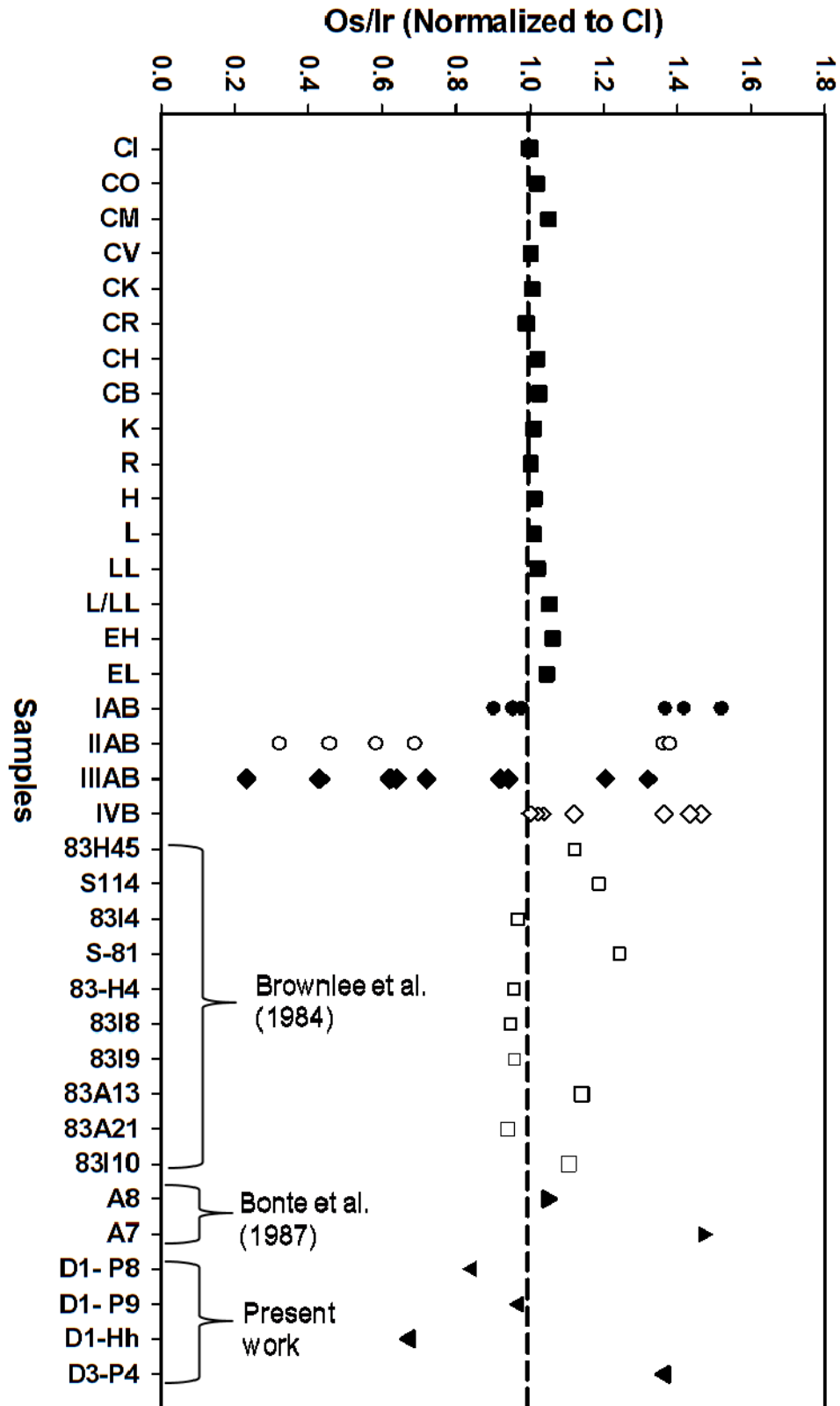


Figure 10

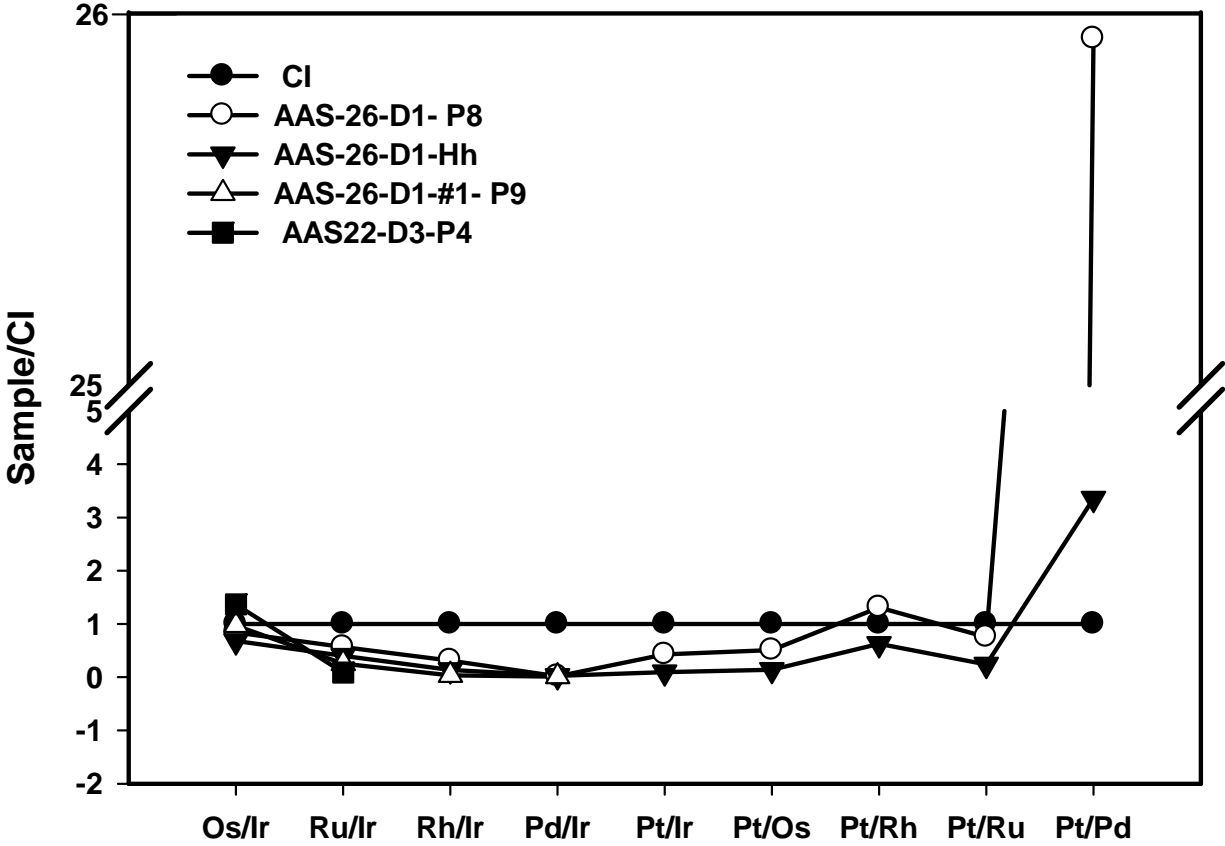


Table 1: Statistics of the sample collected and characterized for their types. The number of cosmic spherules where nuggets were found.

	No. of CS	I-type	S-type	G-type	Nugget observed
AAS26-D1	79	49	18	5	7
AAS26-D2	6	5	-	-	1
AAS26-D3	19	10	6	3	-
AAS26-D4	44	20	19	5	-
AAS26-D5	33	15	17	1	-
AAS26-D6	28	14	11	3	-
AAS22-D1	14	3	11	-	-
AAS22-D3	36	14	17	1	4
AAS22-D7	11	3	7	1	-
AAS22-D8	43	12	29	2	-
AAS22-D10	38	14	22	2	-
AAS-38-139	27	3	23	0	1
Total	378	162	180	23	13

Table 2: Statistical detail of cosmic spherule where platinum group element of both micrometer and nanometer sized nuggets were found.

Sample details	No. of nanometer sized nuggets	No. of micrometer sized nuggets
AAS-26-D1-#2- P1	104	-
AAS-26-D1-#1- P8	1	-
AAS-26-D2-#1- P2	36	-
AAS-26-D1- P8	5	1
AAS26-D1-# 4(A)-P 4	1	-
AAS-26-D1-#2- P5	1	-
AAS-26-D1-#1- P9	-	1
AAS-26-D1-Hh	-	1
AAS-22-D3-P3	20	-
AAS-22-D3-P4	6	1
AAS-22-D3-P11	16	-
AAS-22-D3-P13	22	-
AAS38-139-#1-P20	1	-
Total No.	213	4
Average size	273 nm	4.1 $\mu\text{m}$
Maximum size	762 nm	4.9 $\mu\text{m}$
Minimum size	93 nm	3.3 $\mu\text{m}$

Table 3: Platinum group element data from micrometer sized nuggets of cosmic spherules along with size of nuggets and spherules.

	AAS-26-D1#1-P8	AAS-26-D1-#1- P9	AAS-26-D1-Hh	AAS22-D3-P4
Size of spherule ( $\mu\text{m}$ )	266	273	284	180
Size of nugget ( $\mu\text{m}$ )	4.9	4.5	3.3	3.6
Fe	17.7	9.5	11.1	8.9
Ni	5.0	1.0	2.9	0.5
Ru	17.6	14.5	19.9	4.4
Rh	1.9	0.2	1.4	-
Pd	0.4	0.5	1.1	-
Os	18.3	38.4	23.5	50.8
Ir	20.5	37.3	32.8	35.0
Pt	17.7	-	6.4	-
Total	99.1	101.2	99.0	99.7

Table 4: Platinum group element data of nanometer sized nuggets from the cosmic spherules where  $\mu\text{m}$  size nuggets are present.

Spherule No. (Size)	Nugget No.	Size (nm)	Fe	Ni	Ru	Rh	Pd	Os	Ir	Pt
AAS26-D1#1-P8 266 $\mu\text{m}$	1	305	89.5	9.1	-	0.3	-	-	-	2.4
	2	109	93.9	7.8	0.2	0.6	-	-	-	4.9
	3	275	85.6	8.2	-	0.8	-	-	-	6.4
	4	278	91.7	8.6	-	0.7	-	-	-	4.3
	5	304	89.0	11.6	-	0.6	-	-	-	4.8
AAS22-D3-P4 180 $\mu\text{m}$	1	661	96.4	-	-	-	-	-	-	2.6
	2	702	99.5	-	-	-	-	-	-	1.5
	3	545	92.6	-	-	-	-	-	-	5.4
	4	762	95.0	-	-	-	-	-	-	3.0
	5	366	91.9	0.6	-	-	-	-	-	7.5
	6	455	95.5	-	-	-	-	-	-	2.5

Table 5: Ratios of platinum group compared with CI for micrometer sized nuggets.

	CI*	AAS-26-D1- P8	AAS-26-D1-#1- P9	AAS-26-D1-Hh	AAS22-D3-P4
Os/Ir	1.06	0.89	1.03	0.72	1.45
Ru/Ir	1.52	0.86	0.39	0.61	0.13
Rh/Ir	0.29	0.09	0.01	0.04	-
Pd/Ir	1.19	0.02	0.01	0.03	-
Pt/Ir	2.03	0.87	-	0.19	-
Pt/Os	1.91	0.97	-	0.27	-
Pt/Rh	7.12	9.32	-	4.46	-
Pt/Ru	1.34	1.01	-	0.32	-
Rh/Ir	0.29	0.09	0.01	0.04	-
Pt/Pd	1.70	44.08	-	5.70	-

\*Tagle and Berlin, 2008



Appendix 1: Sub-micrometer sized nugget data from cosmic spherules.

Spherule No. (Size)	Nugget No.	Size (nm)	Fe	Ni	Ru	Rh	Pd	Os	Ir	Pt
AAS26-D1-#2-P1 258 $\mu\text{m}$	1	373	82.4	5.0	-	1.8	-	-	-	10.9
	2	334	82.3	4.5	-	1.0	-	-	-	10.2
	3	305	85.0	4.0	-	1.3	-	-	-	8.7
	4	261	87.4	4.6	-	0.8	-	-	-	6.6
	5	185	90.1	3.8	-	0.8	-	-	-	5.1
	6	259	84.4	11.3	-	-	-	-	-	3.5
	7	117	89.2	9.9	-	-	-	-	-	2.9
	8	195	88.2	6.7	-	0.5	-	-	-	4.9
	9	152	90.5	6.1	-	0.5	-	-	-	3.3
	10	208	95.8	4.0	-	0.7	-	-	-	4.8
	11	182	96.9	3.3	-	-	-	-	-	2.5
	12	165	90.5	4.2	-	0.6	-	-	-	5.4
	13	233	86.1	10.1	-	0.7	-	-	-	5.7
	14	200	87.2	5.6	0.4	1.1	-	-	-	8.8
	15	167	90.0	5.0	-	0.4	0.3	-	-	4.6
	16	95	92.0	5.1	-	0.6	-	-	-	2.8
	17	234	85.9	7.3	0.3	0.8	0.3	0.3	-	6.1
	18	116	88.4	6.2	-	0.4	-	-	-	2.1
	19	113	86.6	6.8	-	-	-	-	-	2.7
	20	268	86.0	6.9	0.6	1.1	-	-	-	8.1
	21	126	91.9	3.3	-	0.4	-	-	-	3.0
	22	98	93.2	3.6	0.3	0.4	-	-	-	3.1
	23	225	89.5	4.7	0.3	0.9	-	-	-	5.7
	24	149	96.3	2.9	-	0.4	-	-	-	1.8
	25	119	94.5	3.2	-	-	-	-	-	1.3
	26	214	92.8	3.6	-	0.5	-	-	-	3.9
	27	275	93.8	3.5	-	0.3	-	-	-	3.1
	28	147	93.8	4.5	-	0.4	-	-	-	2.2
	29	160	94.2	4.7	-	0.7	-	-	-	3.4
	30	140	96.4	3.8	-	-	-	-	-	1.1
	31	255	89.6	7.0	-	0.3	-	-	-	6.0
	32	177	90.7	5.1	-	-	-	-	-	3.7
	33	178	87.1	5.4	-	0.6	-	-	-	4.4
	34	164	95.9	5.1	0.3	0.4	-	-	-	2.3
	35	212	89.5	6.0	-	0.5	-	-	-	4.6
	36	237	88.9	6.1	-	0.4	-	-	-	6.4
	37	259	87.6	7.7	-	0.8	-	-	-	8.3
	38	214	90.4	5.0	2.2	-	0.4	-	-	1.8
	39	176	90.5	4.6	-	0.4	-	-	-	3.9
	40	200	91.8	4.4	-	0.3	-	-	-	5.8
	41	182	89.7	4.8	-	-	-	-	-	2.8
	42	219	95.0	3.9	-	0.6	0.2	-	-	2.1
	43	273	92.5	5.3	-	0.3	-	-	-	2.3

44	388	83.4	5.0	0.5	1.2	0.3	-	-	9.8
45	380	90.6	3.6	-	0.6	0.2	-	-	4.0
46	323	94.6	2.9	-	0.3	-	-	-	2.3
47	163	95.2	3.1	0.2	0.3	-	-	-	1.8
48	485	89.4	4.4	0.3	1.0	-	-	-	9.6
49	427	81.0	10.3	0.3	1.0	0.4	-	-	6.3
50	403	90.2	5.1	0.2	0.8	0.4	-	-	4.0
51	227	95.1	3.9	0.2	0.6	-	-	-	5.3
52	215	92.6	6.2	-	-	-	-	-	2.8
53	201	96.7	3.5	-	0.5	0.2	-	-	2.7
54	236	89.5	4.4	-	0.9	-	-	-	6.7
55	205	94.5	4.8	-	0.4	-	-	-	3.2
56	179	92.5	5.2	-	-	-	-	-	1.9
57	233	90.5	4.6	-	-	-	-	-	2.3
58	278	92.7	4.6	-	0.3	-	-	-	4.4
59	353	82.3	7.0	-	0.7	-	-	-	11.9
60	329	90.9	5.0	0.2	0.5	0.2	-	-	4.2
61	184	90.9	5.2	-	0.5	-	-	-	4.5
62	168	97.6	2.8	-	0.2	-	-	-	1.1
63	242	86.3	5.3	0.2	1.4	-	-	-	10.7
64	221	90.7	5.6	0.3	1.1	-	-	-	5.4
65	241	92.3	4.1	-	0.3	-	-	-	5.1
66	286	84.9	10.3	0.3	0.9	-	-	-	7.3
67	324	84.4	5.6	0.2	1.3	-	-	-	11.7
68	193	94.2	4.4	-	0.4	-	-	-	3.5
69	259	92.4	4.6	-	0.3	-	-	-	3.2
70	327	85.7	6.6	-	0.7	-	-	-	7.8
71	222	86.0	6.9	-	0.4	-	-	-	6.5
72	226	89.6	6.3	0.2	0.6	-	-	-	4.8
73	247	93.6	3.5	0.2	0.4	-	-	-	2.4
74	171	95.3	3.2	-	-	0.2	-	0.2	1.4
76	240	88.3	6.1	-	0.6	-	-	-	5.8
77	340	86.5	5.0	-	0.5	-	-	-	5.5
78	336	93.1	5.7	-	0.4	0.2	-	-	3.2
79	316	85.1	7.0	0.3	0.9	-	-	-	9.4
80	265	89.6	4.9	-	0.4	-	-	-	6.1
81	345	90.9	5.1	-	0.4	-	-	-	5.2
82	408	88.4	6.7	-	0.8	-	-	-	8.9
83	230	96.7	3.6	-	-	-	-	-	2.3
84	277	95.3	3.9	-	0.6	-	-	-	4.6
85	310	96.0	3.5	0.2	0.3	-	-	-	1.7
86	268	90.8	5.2	-	0.8	0.2	-	-	6.3
87	284	93.7	3.8	-	0.5	-	-	-	4.0
88	173	97.0	3.5	-	0.3	-	-	-	1.6
89	351	79.7	5.3	0.3	1.6	-	0.3	-	13.2
90	256	84.6	5.0	0.2	1.0	-	0.2	-	9.5

91	202	92.0	3.0	-	0.4	-	-	-	3.1
92	272	94.0	3.3	0.4	0.5	-	-	-	4.2
93	272	89.3	4.4	0.2	0.9	0.2	-	-	7.1
94	179	94.2	4.0	-	0.2	-	-	-	2.2
95	397	82.4	5.6	0.2	1.2	-	-	-	13.1
96	282	89.9	5.0	-	0.9	0.2	-	-	6.4
97	279	87.4	5.8	0.2	1.2	0.2	-	-	9.4
98	229	91.3	5.5	-	0.5	-	-	-	4.4
99	177	95.3	2.9	-	0.4	-	-	-	1.3
100	243	95.0	4.5	-	0.4	-	-	-	4.4
101	212	92.3	4.3	-	0.5	-	-	-	3.4
102	283	90.9	5.7	-	0.3	-	-	-	4.4
103	250	89.9	6.5	0.2	0.7	-	-	-	4.5
104	187	91.2	4.9	-	-	0.2	-	-	3.1
<hr/>									
AAS26-D1-P8	1	489	86.1	7.4	-	1.2	-	-	8.2
<hr/>									
268 $\mu\text{m}$									
<hr/>									
AAS26-D2-#1-P2	1	334	84.3	8.5	0.3	1.1	-	-	9.5
<hr/>									
260 $\mu\text{m}$	2	264	91.5	5.3	0.2	0.6	-	-	5.1
	3	202	86.5	9.3	-	0.9	-	-	9.8
	4	349	80.9	7.5	-	1.4	-	-	13.7
	5	318	76.6	11.9	-	1.7	-	-	16.1
	6	434	78.0	12.8	-	1.5	-	-	11.5
	7	239	89.0	7.5	0.2	0.4	-	-	7.6
	8	270	94.9	4.6	-	0.2	-	-	5.0
	9	275	95.3	4.5	-	0.6	-	-	3.9
	10	224	82.0	16.8	-	0.5	-	-	6.2
	11	202	91.7	5.9	-	0.6	-	-	5.2
	12	187	89.5	12.8	-	0.5	-	-	2.6
	13	184	78.6	9.6	-	1.6	-	-	14.9
	14	208	96.0	4.5	-	0.4	-	-	4.0
	17	211	93.6	6.8	-	0.8	-	-	6.6
	18	204	93.8	4.8	-	0.4	-	-	3.0
	19	266	95.8	4.8	-	0.3	-	-	2.9
	20	321	90.2	5.7	-	0.4	-	-	7.0
	21	304	87.4	7.1	-	0.9	-	-	9.6
	22	192	98.9	4.8	-	0.2	-	-	2.8
	23	409	76.6	11.8	0.3	1.5	-	-	15.1
	24	370	71.2	10.0	-	1.6	-	-	20.8
	25	211	83.0	9.0	-	1.2	-	-	10.6
	26	220	90.3	6.3	0.2	0.8	-	-	4.7
	27	223	88.7	5.4	-	0.7	-	-	6.7
	29	196	93.2	3.1	-	0.3	-	-	1.8
	30	280	91.8	4.8	-	0.2	-	-	2.2
	31	307	86.1	6.8	-	0.8	-	-	6.9
	32	257	87.9	6.8	-	0.5	-	-	6.5
	33	214	91.2	5.5	-	0.6	-	-	5.8

	34	225	91.9	6.0	-	0.8	-	-	-	7.8
	35	385	77.3	10.2	0.4	1.6	-	-	-	13.7
	36	280	77.0	16.2	-	0.5	-	-	-	7.8
AAS26-D1#1-P8	1	305	89.5	9.1	-	0.3	-	-	-	2.4
266 $\mu\text{m}$	2	109	93.9	7.8	0.2	0.6	-	-	-	4.9
	3	275	85.6	8.2	-	0.8	-	-	-	6.4
	4	278	91.7	8.6	-	0.7	-	-	-	4.3
	5	304	89.0	11.6	-	0.6	-	-	-	4.8
AAS26-D1-#4(A)-P4	1	240	88.6	8.1	-	0.5	-	-	-	2.8
64 $\mu\text{m}$										
AAS38-139-#1-P20	1	553	57.7	32.0	-	1.0	-	2.0	-	9.8
320 $\mu\text{m}$										
AAS26-D1-#2-P5	1	550	87.4	11.5	-	0.3	-	-	-	4.9
226 $\mu\text{m}$										
AAS22-D3-P3	1	638	91.4	6.1	-	-	-	-	-	1.8
212 $\mu\text{m}$	2	500	92.0	5.1	-	-	-	-	-	1.3
	3	648	91.1	3.2	-	-	-	-	-	4.4
	4	457	91.5	4.3	-	-	-	-	-	2.8
	5	529	90.2	3.1	-	-	-	-	-	5.4
	6	209	90.0	4.6	-	-	-	-	-	3.9
	7	220	87.0	7.0	-	-	-	-	-	5.2
	8	211	86.3	5.2	-	-	-	-	-	4.9
	9	201	91.3	4.3	-	-	-	-	-	5.9
	10	138	90.2	4.7	-	-	-	-	-	3.0
	11	93	93.6	2.8	-	-	-	-	-	1.0
	12	205	91.9	4.0	-	-	-	-	-	4.4
	13	200	90.6	3.9	-	-	-	-	-	2.6
	14	202	91.5	3.6	-	-	-	-	-	3.1
	15	114	91.2	4.0	-	-	-	-	-	1.2
	16	337	90.2	3.9	-	-	-	-	-	3.5
	17	412	91.7	4.3	-	-	-	-	-	1.7
	18	224	94.0	2.2	-	-	-	-	-	0.5
	19	260	96.4	2.1	-	-	-	-	-	0.3
	20	155	95.1	3.0	-	-	-	-	-	0.4
AAS22-D3-P4	1	661	96.4	-	-	-	-	-	-	2.6
180 $\mu\text{m}$	2	702	99.5	-	-	-	-	-	-	1.5
	3	545	92.6	-	-	-	-	-	-	5.4
	4	762	95.0	-	-	-	-	-	-	3.0
	5	366	91.9	0.6	-	-	-	-	-	7.5
	6	455	95.5	-	-	-	-	-	-	2.5
AAS22-D3-P11	1	214	83.9	6.9	-	0.9	-	-	-	10.4
202 $\mu\text{m}$	2	278	80.9	7.8	-	0.9	-	-	-	10.4
	3	183	88.0	6.2	-	-	-	-	-	3.8
	4	505	87.1	5.9	-	-	-	-	-	5.3

	5	250	91.3	6.0	-	-	-	-	-	1.3
	6	334	83.5	10.3	-	-	-	-	-	3.7
	7	234	89.5	4.5	-	-	-	-	-	5.0
	8	170	91.2	4.5	-	-	-	-	-	3.5
	9	273	91.3	3.6	-	0.6	-	-	-	2.5
	10	303	89.0	9.3	-	-	-	-	-	1.2
	11	431	88.1	10.0	-	-	-	-	-	1.0
	12	346	91.0	8.2	-	-	-	-	-	0.2
	13	647	90.2	4.4	-	-	-	-	-	4.8
	14	455	90.4	5.0	-	-	-	-	-	2.5
	15	239	91.6	4.0	-	-	-	-	-	2.4
	16	218	91.4	7.7	-	-	-	-	-	0.9
<hr/>										
AAS22-D3-P13	1	348	90.1	0.7	-	-	-	-	-	9.1
361 $\mu\text{m}$	2	151	96.2	-	-	-	-	-	-	3.6
	3	427	83.6	0.8	-	0.8	-	-	-	15.2
	4	202	95.2	0.5	-	-	-	-	-	4.0
	5	465	73.9	0.8	-	1.7	-	-	-	24.2
	6	424	81.7	0.8	-	0.9	-	-	-	16.8
	7	190	93.1	0.5	-	-	-	-	-	6.0
	8	270	98.0	-	-	-	-	-	-	1.5
	9	210	95.3	-	-	-	-	-	-	2.9
	10	248	94.8	0.7	-	-	-	-	-	2.3
	11	250	95.4	0.5	-	-	-	-	-	1.3
	12	263	88.4	0.6	-	-	-	-	-	9.0
	13	137	90.1	0.6	-	-	-	-	-	7.7
	14	417	87.5	0.8	-	-	-	-	-	9.7
	15	298	93.7	-	-	-	-	-	-	3.3
	16	281	91.4	-	-	-	-	-	-	6.3
	17	236	92.0	0.8	-	-	-	-	-	6.7
	18	260	91.9	-	-	-	-	-	-	6.1
	19	186	96.2	-	-	-	-	-	-	1.0
	20	234	92.3	0.5	-	-	-	-	-	5.1
	21	148	96.5	-	-	-	-	-	-	1.9
	22	196	98.2	-	-	-	-	-	-	0.3
<hr/>										
	Average	272.7	90.3	5.6	-	0.6	-	-	-	5.3
	Stdev	117.1	5.5	3.4	-	0.4	-	-	-	3.8
	Error	8.1	0.4	0.2	-	-	-	-	-	0.3
<hr/>										